International Journal of Nanomedicine Dovepress

Open Access Full Text Article ORIGINAL RESEARCH

Dextran-Graft-Polyacrylamide/Zinc Oxide Nanoparticles Inhibit of Cancer Cells in vitro and in vivo

Petro Virych[1], Pavlo Virych[2], Volodymyr Prokopiuk[3,4], Anatolii Onishchenko[3], Mykola Ischenko[2], Volodymyr Doroschuk[2], Valentyna Kurovska[5], Anton Tkachenko[4], Nataliya Kutsevol[2]

[1]Laboratory of Mechanisms of Drug Resistance, R.E. Kavetsky Institute for Experimental Pathology, Oncology and Radiobiology, Kyiv, Ukraine; [2]Faculty of Chemistry, Taras Shevchenko National University of Kyiv, Kyiv, Ukraine; [3]Research Institute of Experimental and Clinical Medicine, Kharkiv National Medical University, Kharkiv, Ukraine; [4]Department of Cryobiochemistry, Institute for Problems of Cryobiology and Cryomedicine of the National Academy of Sciences of Ukraine, Kharkiv, Ukraine; [5]Educational and Scientific Center "Institute of Biology and Medicine", Taras Shevchenko National University of Kyiv, Kyiv, Ukraine

Correspondence: Pavlo Virych, Faculty of Chemistry, Taras Shevchenko National University of Kyiv, 60 Volodymyrska str, Kyiv, 01601, Ukraine, Email pavlo.virych@knu.ua; Anton Tkachenko, Department of Cryobiochemistry, Institute for Problems of Cryobiology and Cryomedicine of the National Academy of Sciences of Ukraine, 23 Pereyaslavskaya St, Kharkiv, 61015, Ukraine, Email as.tkachenko@knmu.edu.ua

Introduction: Tumor drug resistance and systemic toxicity are major challenges of modern anticancer therapy. Nanotechnology makes it possible to create new materials with the required properties for anticancer therapy.

Methods: In this research, Dextran-graft-Polyacrylamide/ZnO nanoparticles were used. The study was carried out using prostate (DU-145, LNCaP, PC-3), breast (MDA-MB-231, MCF-7, MCF-7 Dox) cancer cells and non-malignant (MAEC, BALB/3T3 clone A31) cells. Zinc was visualized with fluorescence in vitro and in vivo. ROS and apoptotic markers were identified by cytometry. Zinc accumulation and histopathological changes in the tumor, liver, kidney, and spleen were evaluated in a rat model.

Results: ZnO nanoparticles dissociation and release of Zn^{2+} into the cytosol occurs in 2–3 hours for cancerous and non-cancerous cells. ROS upregulation was detected in all cells. For non-malignant cells, the difference between the initial ROS level was insignificant. The rate of carbohydrate metabolism in cancer cells was reduced by nanosystems. Zinc level in the tumor was upregulated by 25% and 39% after treatment with nanosystems and doxorubicin combined, respectively. The tumor Walker-256 carcinosarcoma volume was reduced twice following mono-treatment with the nanocomplex and 65-fold lower when the nanocomplex was combined with doxorubicin compared with controls. In the liver, kidney and spleen, the zinc level increased by 10–15% but no significant pathological alterations in the tissues were detected.

Conclusion: D-PAA/ZnO NPs nanosystems were internalized by prostate, breast cancer cells and non-malignant cells via endocytosis after short time, but cytotoxicity against non-cancer cells were significantly lower in vitro and in vivo. D-PAA/ZnO NPs nanocomplex efficiently promoted cell death of tumor cells without showing cytotoxicity against non-malignant cells making it a promising anti-cancer agent.

Keywords: zinc oxide nanoparticles, doxorubicin, prostate cancer, breast cancer, zinc imaging, histopathology

Introduction

The last few decades have witnessed significant advances in nanotechnology. The organization of materials into nanoscale structures noticeably changes their properties. Nanosize-mediated characteristics allow nanoparticles to interact with cellular structures in a special way.[1] All nanomaterials have a large surface area-to- volume ratio, which significantly increases their reaction properties. Despite significant progress in nanomedicine, our knowledge of intricate mechanisms that govern interactions between nanomaterials, cells and tissues are still ambiguous.[2]

Zinc oxide nanoparticles (ZnO NPs) have semiconductor properties, which allow them to be applied in electronics, optics, photocatalysis, cosmetics, and medicine.[3] There is abundant evidence that zinc is low-toxic to cells at

Received: 14 August 2024
Accepted: 3 November 2024
Published: 11 November 2024

physiological conditions (pH = 7.4).[4] ZnO NPs have a high biocompatibility due to weak dissociation and Zn^{2+} release. Nevertheless, it has been reported that ZnO NPs cause oxidative stress and cell damage at slightly acidic pH. Tumor cells stimulate significant changes in environmental tissues. Tumor microenvironment (TME) of various cancer types is different, but hallmark features include blood vessels, immune cells and extracellular matrix. The TME dynamically changes in response to hypoxia and decreased pH. The Warburg effect promotes the production of lactate and its efflux into the intercellular space.[5] This significantly reduces the effectiveness of anticancer pharmaceuticals. In addition, TME cells initiate a program of active angiogenesis to remove metabolites and supply the tumor with oxygen and nutrients. Thus, based on the TME parameters, ZnO NPs can accumulate and interact with the tumor with some selectivity due to greater blood flow and low pH[3].

Importantly, ZnO NPs interact with biomolecules to form a dynamic protein corona.[6] The complex is recognized by immune cells and can be phagocytosed by macrophages. Analysis of nanocarrier/ZnO NPs distribution in tissues is important for identifying target organs, features of accumulation and specific toxicity.[7] Of note, the distribution of ZnO NPs in organs strongly depends on exposure route and physicochemical properties.[8] ZnO NPs do not cause significant pathological changes in the kidneys, brain and spleen, but their hepatotoxicity has been reported.[9] As an approach to partially prevent opsonization and reduce the cytotoxicity of ZnO NPs, their conjugation with polymer nanocarriers can be used.[10] Since the polymer-nanocarrier complex can provide targeted delivery to tumors,[11] these nanosystems have significantly higher bioavailability, tumor-damaging capacity and selectivity compared to free ZnO NPs.

Most human tumors are characterized by increased glucose consumption compared to the surrounding tissues. Glucose is metabolized to lactate, known as the Warburg effect.[12] It should be emphasized that this phenomenon favors the growth and invasion of tumors, especially under hypoxic conditions. Excessive lactic acid is exported from the cells through H+/lactate symporters MCT1/MCT4.[13–15] Notably, environmental acidification has a toxic effect on normal cells and interferes with the influx of anticancer drugs.[16]

Polymer nanocarriers are important for improving bioavailability of pharmaceuticals and safeguard healthy cells from toxic effects of certain therapeutics. Polymer carriers can deliver different type of biologically active substance, for example, small molecules, peptides, genes, RNA, metal nanoparticles etc. Other important properties are stabilization and increase of drugs bioavailability.[17] ZnO NPs are prone to aggregation with subsequent loss of activity. Therefore, a star-like copolymer dextran-polyacrylamide was used to prevent aggregation and increase bioavailability of the nanosystem. The main advantages of such star-like polymers as nanocarriers and scaffolds for encapsulation of drugs, small organic molecules as well as inorganic nanoparticles are related to the internal structure of star-like molecules. They have more rigid structure in comparison with linear polymer using now. Star-like molecules almost do not change their conformation (size) after encapsulation of some substances inside of molecules because grafted polyacrylamide chains in branched structure have limited flexibility. For biomedical application namely size and functionality of polymer nanocarrier play the main role.

A number of earlier studies have demonstrated that dextran-graft-polyacrylamide (D-PAA) polymers are of low toxicity.[18,19] Moreover, D-PAA/ZnO NPs have been shown to be of mild toxicity to non-cancer and blood cells.[20,21] Additionally, experimental evidence indicates that apoptosis is induced and adhesion proteins are overexpressed in prostate and breast cancer cells exposed to D-PAA/ZnO NPs. Thus, despite some evidence that D-PAA/ZnO NPs nanosystems can be considered as promising anti-cancer agents, more cell culture-based and animal studies are required to unveil their effects.

The aim of the research was to determine the anticancer properties of D-PAA/ZnO NPs in cell models of breast and prostate cancer in vitro, as well as the possibility of tumor inhibition in vivo. For this purpose, we have studied the dynamics D-PAA/ZnO NPs-derived of intracellular zinc accumulation in prostate and breast cancer cells with distinct physiological features of intracellular zinc regulation. Additionally, we determined the intracellular ROS-levels, phosphatidylserine externalization, features of glucose metabolism and lactate production to delve into the molecular mechanisms of D-PAA/ZnO NPs-induced anti-cancer effects. Finally, we intended to determine the zinc accumulation and histopathological changes in the liver, kidney, spleen and tumor in an in vivo model following D-PAA/ZnO NPs cancer treatment.

Materials and Methods

Synthesis and Macromolecular Parameters of Dextran-Graft-Polyacrylamide/ZnO Nanoparticles

All chemicals were Fluka (Buchs, Switzerland). A star-like dextran-graft-polyacrylamide copolymer was used. The polymers were synthesized in an argon atmosphere at room temperature for 24 h. Cerium-ion-induced redox initiation method was used. Polyacrylamide was grafted to Dextran backbone. The average number of polyacrylamide arms is 10, Mn = $8.6 \cdot 10^5$ g·mole^{-1} and the polydispersity index is Mw/Mn = 1.62. The route of synthesis, characterization and peculiarities of copolymer structure were reported earlier.[22] ZnO NPs were synthesized in D-PAA matrices by precipitation method. Initially, 1 mL of a $ZnSO_4$ solution (0.1 mol·mL^{-1}) was added to 5 mL of an aqueous D-PAA solution (10^3 g·mL^{-1}). After 20 minutes, 2 mL of a sodium hydroxide solution (0.1 mol·mL^{-1}) was added dropwise. Solution was then continuously stirred at 50°C for 24 hours to yield D-PAA/ZnO NPs. Synthesis and characterization of ZnO NPs from $ZnSO_4$ in situ into the D-PAA matrix was reported in details earlier as well.[20] The average diameter of ZnO NPs was 3 nm, hydrodynamic radius of D-PAA/ZnO NPs was 7 nm.

Zinc Accumulation in Cells in vitro

The study was carried out using prostate (DU-145, LNCaP, PC-3), breast (MDA-MB-231, MCF-7, MCF-7 Dox) cancer cells and non-malignant (MAEC, BALB/3T3 clone A31 (further 3T3 A31)) cells. Reference cultures were kindly provided by the R.E. Kavetsky Institute of Experimental Pathology, Oncology and Radiobiology, National Academy of Science of Ukraine. Cells were cultured on coverslips in DMEM (Biowest, France) supplemented with 10% fetal bovine serum (Sigma-Aldrich, USA), 40 μg/mL gentamicin, 5% CO_2 atmosphere at 37°C for 48 hours. D-PAA/ZnO NPs nanosystems were added to the incubation solution at EC50 concentrations for each cell line.[20] Non-malignant cells BALB/3T3 clone A31 and MAEC were incubated with 3 mM D-PAA/ZnO NPs. Zinc content was measured at 15-minute intervals during the first hour of incubation, then at one-hour intervals up to 5 hours. After incubation, the glass with cells was washed with saline solution for 30 sec. N-(6-methoxy-8-quinolinyl)-4-methylenebenzenesulfonamide (TSQ, Sigma-Aldrich, USA) was used to determine the zinc content in the cells.[23,24] The dye stock solution was prepared in DMSO. The final concentration of TSQ was 30 μM in phosphate-saline buffer (PBS, Biowest). The cells were incubated in the TSQ solution for 30 min. The dye was washed out with saline solution for 30 sec. Fluorescence was acquired using an Olympus BX53 (Tokyo, Japan) microscope equipped with an XCite Series 120 Q fluorescent block and an Olympus DP72 camera. Fluorescence excitation was performed by an ultraviolet light filter, whereas emission was collected by a blue light filter. Exposure was 10 ms. At least 20 fields of view were snapped for each sample. Testing and luminescence registering were performed under the same conditions for all cells. Experiments were carried out in triplicate.

Cell images processing was carried out with the ImageJ software (Bethesda, Maryland, USA). Integrate density of individual cells was measured. The measured area was 354 μm^2, which corresponds to the area of an individual cell. Integrate density was determined for 100 individual cells. Data were presented as the median and interquartile range (median (Me), 25–75%).

ICP-MS for Zinc Content in Cells

For mineral analysis, 0.5 mL of samples were transferred into PTFE tubes, 0.5 mL of concentrated 69.5% HNO_3 (Fluka, Buchs, Switzerland) was added and the tubes were heated in an oven at 200 °C for 20 min (close to dryness).

After digestion, the solutions were diluted to a final volume of 10 mL. Zinc content was measured by inductively coupled plasma - optical emission spectrometry (ICP-OES) using a spectrometer with axial viewed plasma (Thermo Fisher Scientific iCAP 7000 DUO). Operating conditions were as follows: power of 1150 W; plasma flow gas of 15 L/min; auxiliary gas flow of 0.5 L/min; nebulizer gas flow of 0.5 L/min. All analyses were performed in duplicate.

The selected emission line (213.8 nm) was that providing the maximum signal-to-noise ratio and minimum spectral interferences. Blank correction was performed analyzing reagent blank. The calibration curve was built by analyzing six

standard solutions containing the target metal within the concentration range of 0.01–0.5 mg/L. Instrumental limit of detection, calculated according to [ISO 11843–2:2000] was 0.009 mg/L and the limit of quantitative determination (LoQ) was 0.017 mg/L. All analyzed samples showed results above LoQ.

Cell Lines and Incubation Conditions

Non-malignant murine fibroblasts BALB/3T3 clone A31 and mouse aortic endothelial cells (MAECs), prostate cancer (DU-145, LNCaP, PC-3) and breast cancer cell lines (MCF-7, MCF-7 Dox, MDA-MB-231) were used to assess cell death-promoting effects of the D-PAA/ZnO NPs nanocomplex. The cells were cultured in 24-well plates in DMEM Dulbecco's Modified Eagle Medium (BioWest) supplemented with 10% fetal bovine serum (FBS, BioWest) and 100 U/mL Penicillin/Streptomycin (Thermo Fischer Scientific, USA) at 37 °C and 5% CO_2. Initially, 2×10^5 cells were seeded. The cells were incubated for 24 h with the D-PAA/ZnO NPs nanocomplex at EC30 (DU-145 – 1.82 mM, LNCaP – 2.7 mM, PC-3 – 1.96 mM, MCF-7 – 1.98 mM, MCF-7 Dox – 1.98 mM, MDA-MB-231 – 1.1 mM, respectively). Non-malignant cells BALB/3T3 clone A31 and MAECs were incubated with 3 mM D-PAA/ZnO NPs.

Annexin V/7-Aminoactinomycin D Staining

The cells were collected, washed and stained with annexin V-FITC (BD Pharmingen™ FITC-Annexin V, BD Biosciences, USA), or the combined annexin V-FITC and 7-AAD (7-aminoactinomycin D, BD Pharmingen™, BD Biosciences, USA) staining was employed. The cells were resuspended in 1x Annexin-binding buffer (BD Pharmingen™, BD Biosciences, USA). Following addition of 5 µL of annexin V-FITC or/and 5 µL of 7-AAD, the suspensions of normal and cancer cells were incubated in the dark for 15 min. Detection of fluorescence was performed by BD FACS Canto II flow cytometer (Becton Dickinson, USA). Post-acquisition analysis was carried out using FlowJo (v10; BD Biosciences, USA) software. The difference was considered statistically significant at $p < 0.05$. The experiments were performed in triplicate.

ROS Detection

For ROS level detection, 0.5×10^6 cells were resuspended in 0.5 mL of 15 µM of 2′,7′-dichlorofluorescein diacetate (Sigma Aldrich, USA) and incubated for 40 minutes at 37 °C. Cells were washed with 1.5 mL of PBS (Biowest) and centrifuged at 400 g for 10 min. The cells were resuspended in 0.5 mL of PBS and analyzed on a flow cytometer (DxFlex, Beckman Coulter, Brea, California, USA). Fluorescence intensity was analyzed using the FITC channel (light filter 525/40 nm).

At least 25,000 events were analyzed for each sample. Primary data processing was carried out using the CytExpert software. The difference in ROS level was calculated by following formula:

$$D_{ROS} = \frac{F_s}{F_c} * 100, \%$$

where D_{ROS} was the difference in intracellular ROS level, F_c was fluorescence of untreated cells, F_s was fluorescence of D-PAA/ZnO-treated cells.

The experiments were performed in triplicate.

Glucose and Lactate Determination

Cells were incubated in DMEM (Biowest) with 10% fetal bovine serum (Sigma-Aldrich, USA), 40 µg/mL gentamicin, 5% CO_2 atmosphere at 37°C for 24 h. The medium contained D-PAA/ZnO NPs at EC50 concentrations for each cell line, respectively. Following incubation, the complete medium was collected and analyzed for glucose and lactate content. ChemWell 2900 Auto-Analyser with Lactate Assay Kit (Roche, Hoffmann-La Roche, Basel, Switzerland) and Glucose Assay Kit (Roche) were used for L-lactate (mM) and glucose (mM) determination, respectively. Preparation and measurement of samples were done in accordance with the manufacturer's guidelines. Numerical data were presented as the mean and Standard Deviation (M±SD). The experiments were repeated 5 times.

Interaction of D-PAA/ZnO NPs with Blood Serum Proteins

D-PAA/ZnO NPs nanosystems (8 mM) were incubated with a bovine albumin (Sigma) solution (40 mg/mL) in saline for 24 h. The transmission of 530 nm light (T%) was investigated on a Lambda 365 UV spectrophotometer (Perkin Elmer, Waltham, Massachusetts, USA). The same studies were performed with blood serum of rats. Blood was collected and cells were centrifuged at 1300 rpm (Nuve NF200, Ankara, Republic of Türkiye) for 15 min at room temperature. The serum was not diluted. Serum and an aliquot of D-PAA/ZnO NPs in water were added to quartz cuvettes. The final concentrations of ZnO NPs were 4 and 8 mM. The optical transmittance (T%) at 530 nm was measured similarly to the studies with albumin. The experiments were repeated 5 times.

In vivo Studies

The experiment was carried out on Wistar breed rats. The animals were kept under standard conditions in the vivarium of the Institute for Problems of Cryobiology and Cryomedicine NAS of Ukraine. All manipulations with laboratory animals were carried out in accordance with the Law of Ukraine "On the Protection of Animals from Cruelty Treatment", "On Approval of the Procedure for Conducting Experiments and Experiments on Animals by Scientific Institutions", European Convention on the Protection of Vertebrate Animals (Strasbourg, March 18, 1986), Directives of the Council of the European Economic Society on the Protection of Vertebrate Animals (Strasbourg, November 24, 1986) and Helsinki Declaration of the World Medical Association. The research was approved by the Ethics and Bioethics Committee of the Kharkiv National Medical University (Kharkiv National Medical University, Kharkiv, Ukraine; minutes #9 dated November 3, 2021).

Walker-256 carcinosarcoma cells were used to generate tumors. Cell suspension (10^6 cells) in saline was injected subcutaneously into the right side of the rats. The animals were divided into 5 groups containing 5 animals each:

1. Control (saline);
2. D-PAA (1 mg/mL);
3. Doxorubicin (1.5 mg/kg weight);
4. D-PAA/ZnO NPs (200 μMol/kg weight);
5. D-PAA/ZnO NPs (200 μMol/kg weight + Doxorubicin 1.5 mg/kg weight).

All samples (the volume was 0.5 mL) were injected into the lateral tail vein (syringe U-40 BD Micro-Fine Plus 30G, Becton, Dickinson and Company, USA) daily for 5 days. Therapy was administered on day 3 after tumor inoculation. The injection site was treated with 96% ethyl alcohol (MyChem, Kyiv, Ukraine). Following 5 days of therapy, the size of the tumor was measured with a caliper Miol-15-240. The volume of the tumor was calculated in accordance with the following formula:[25]

$$V = \frac{4}{3} \cdot \pi \cdot \frac{l}{2} \cdot \frac{w}{2} \cdot \frac{h}{2}$$

where V is the volume of tumor (cm^3); *l, w* and *h* are width, length and height of tumor, respectively.

On day 5, the animals were decapitated. Kidney, liver, spleen, and tumor samples were collected for determination of the relative zinc content and histopathological studies.

Zinc Content in Tissues

Fragments of hepatic, renal, splenic and tumor tissues were rapidly frozen at −18 °C and histological sections of 20 μm were prepared with Microtome Cryostat HM525 (Microm, Thermo Scientific, Waltham, Massachusetts, USA). The slides with tissue sections were kept at 37 °C for 1 h. Samples were incubated with TSQ (30 μM in PBS) for 30 min at 37 °C. The dye was not washed out. Fluorescence was investigated using an Olympus BX53 microscope equipped with an XCite Series 120 Q fluorescent block and an Olympus DP72 camera. Fluorescence excitation was performed with an ultraviolet light filter, whereas emission was collected with a blue light filter. Exposure was 10 ms, whereas 5 histological sections were analyzed for each tissue sample. Image processing was carried out with the ImageJ software. Integrate

density of the same tissue area (at least 30 plots at 10 histological slides) was measured. Data were presented as the median and interquartile range (median (Me), 25–75%).

Histopathological Studies

The selected rat organs were immediately placed in formal calcium (10% $CaCl_2$ in formaldehyde) and kept for 7 days. Tissue samples were embedded in paraffin blocks. Tissue sections of 5–6 μm were made on a microtome Microm HM325 (Thermo Scientific, Waltham Massachusetts, USA). Histological sections were deparaffinized and stained with hematoxylin-eosin according to standard techniques.[26] Tissue samples were analyzed on an Olympus BX53 (Tokyo, Japan) microscope equipped with an Olympus DP72 camera.

Statistical Analysis

Statistical data processing was carried out using the one-way ANOVA Scheffe test (M±SD, $p<0.05$) for parametric data. Mann–Whitney *U*-test was applied using Graph Pad Prism 5.0 software (USA). Kruskal–Wallis and Dunn's tests were used to compare the non-parametric data. Results were presented as the median and interquartile range (Me, 25–75%). The difference was statistically significant at $p<0.05$.

Results and Discussion

There is accumulating evidence that the zinc level in tissues and blood is considered to be a cancer marker. For instance, zinc levels in breast cancer tissues are higher than in healthy tissues, and reduction of circulating zinc levels has been additionally reported.[27] Notably, prostate cancer tissue has lower levels of zinc than the healthy tissues. Zinc level in blood has been demonstrated to be lower in men with prostate cancer.[28] These changes are associated with impaired expression of zinc transporters and altered regulation of zinc concentration in cells.[29–31] Interestingly, ZnO NPs are a relatively safer source of Zn compared to soluble forms. Uptake and accumulation of NPs by cancer cells is of huge importance for determining the toxicity of ZnO NPs-based nanomaterials.

The basic zinc levels in prostate (DU-145, PC-3, LNCaP), breast (MDA-MB-231, MCF-7, MCF-7 Dox) cancer cell lines and non-malignant (3T3 A31, MAEC) cells are illustrated in Figure 1.

Weak STQ fluorescence in prostate cancer (DU-145, LNCaP) and non-malignant cells (MAEC) was detected. Fluorescence was statistically significantly higher in MCF-7, MCF-7 Dox and MDA-MB-231 breast cancer cells compared to MAEC. Fluorescence of fibroblasts 3T3 A31 and prostate PC-3 cancer cells was found to be elevated. Baseline fluorescence values of the cells are summarized in Supplementary Figure S1. The initial fluorescence levels were chosen as baselines to assess internalization of D-PAA/ZnO NPs and cellular zinc accumulation.

In the current study, we demonstrated that zinc accumulation in 3T3 A31 cells and MAEC was similar. A statistically significant increase in intracellular zinc level was detected after 45 min of incubation with D-PAA/ZnO NPs nanosystems (Figure 2A and B).

We are reporting an increase in cellular granularity. It has been suggested that D-PAA/ZnO NPs are internalized by endocytosis and remain in endocytosis vesicles and lysosomes for some time.[32] Furthermore, uniform fluorescence of the vast majority of 3T3 A31 and MAEC cells was shown after 2–3 h of incubation with D-PAA/ZnO NPs (Supplementary Figures S2 and S3).

These changes could be attributed to the release of Zn^{2+} from lysosomes and its accumulation in the cytoplasm. The maximum intracellular level of zinc was detected following 4 h of incubation. Accumulated zinc was partly unloaded from 3T3 A31 cells after 5 h. This phenomenon was not detected for the MAEC cell line. Nor further accumulation was observed. Thus, different mechanisms for regulating intracellular zinc content were detected in these cell lines.[33] A change in the shape of most cells to spherical was observed after incubation of non-malignant cells with D-PAA/ZnO NPs for 5 h, but there were no visual signs of apoptosis. Thus, non-malignant 3T3 A31 and MAEC cells internalize and accumulate D-PAA/ZnO NPs nanosystems without affecting viability of cells, which has also been demonstrated in our earlier studies.[20,21]

Prostate cancer cells LNCaP, DU-145 and PC-3 internalize D-PAA/ZnO NPs faster than the non-malignant cells (Figure 3).

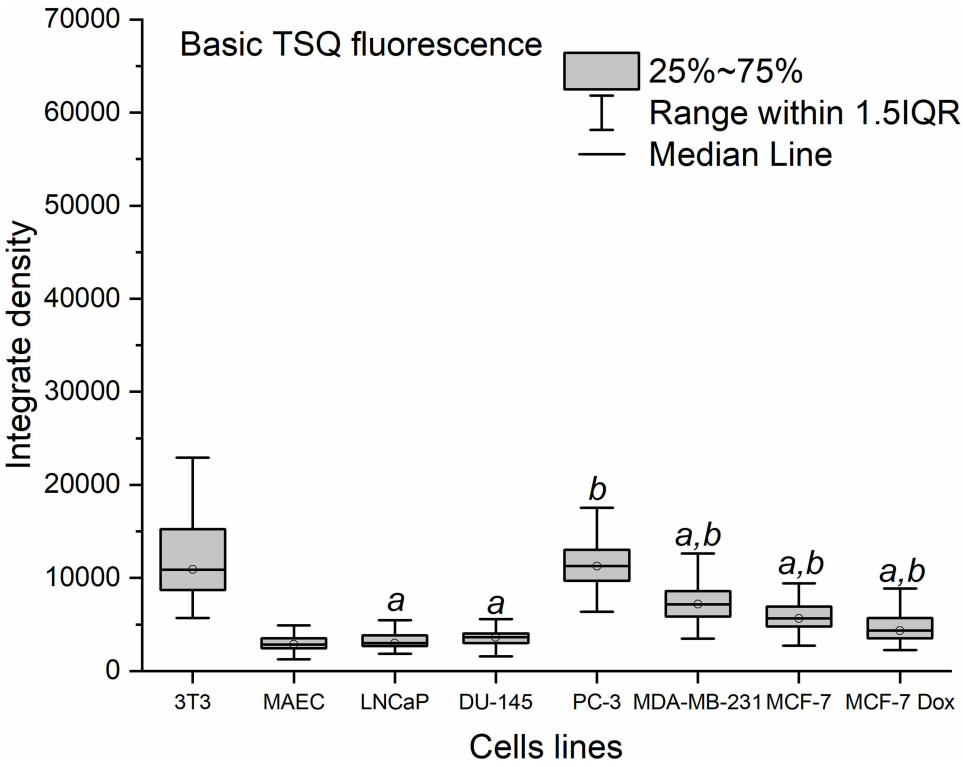

Figure 1 Fluorescence of TSQ in prostate (DU-145, PC-3, LNCaP), breast (MDA-MB-231, MCF-7, MCF-7 Dox) and non-malignant (MAEC, 3T3 A31) cell lines untreated with dextran-graft-polyacrylamide/ZnO nanoparticles (median, 25%-75%; Kruskal–Wallis test: ap < 0.05 compared to 3T3 A31, bp < 0.05 compared to MAEC). Staining with 30 μM TSQ for 30 min.

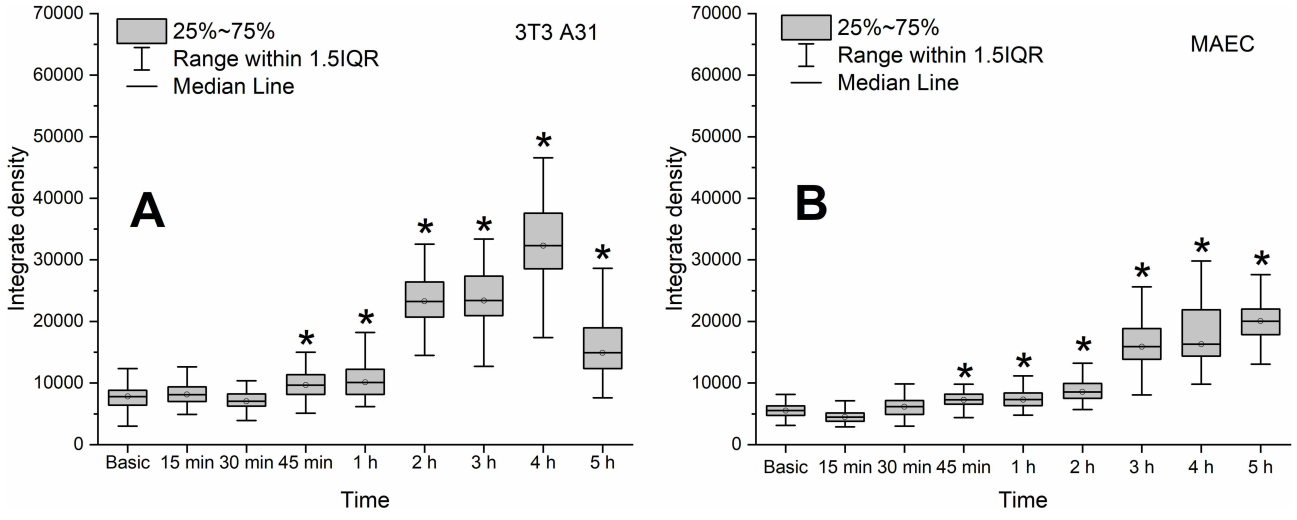

Figure 2 Zinc level in the non-malignant 3T3 A31 (**A**) and MAEC (**B**) cells during their incubation with dextran-graft-polyacrylamide/ZnO nanoparticles (D-PAA/ZnO NPs) for 5 h (median, 25%-75%; Kruskal–Wallis test: *p < 0.05). Basic fluorescence is the fluorescence of cells without D-PAA/ZnO NPs treatment. Staining with 30 μM TSQ for 30 min.

A statistically significant increase in zinc levels in LNCaP and PC-3 cells was detected following 30 min, and DU-145 after 15 min incubation with D-PAA/ZnO NPs. Almost the entire internalized zinc was localized in multiple vesicles, presumably lysosomes. There were significantly more vesicles in prostate cancer cells than in the non-cancerous cells (Supplementary Figures S4–S6).

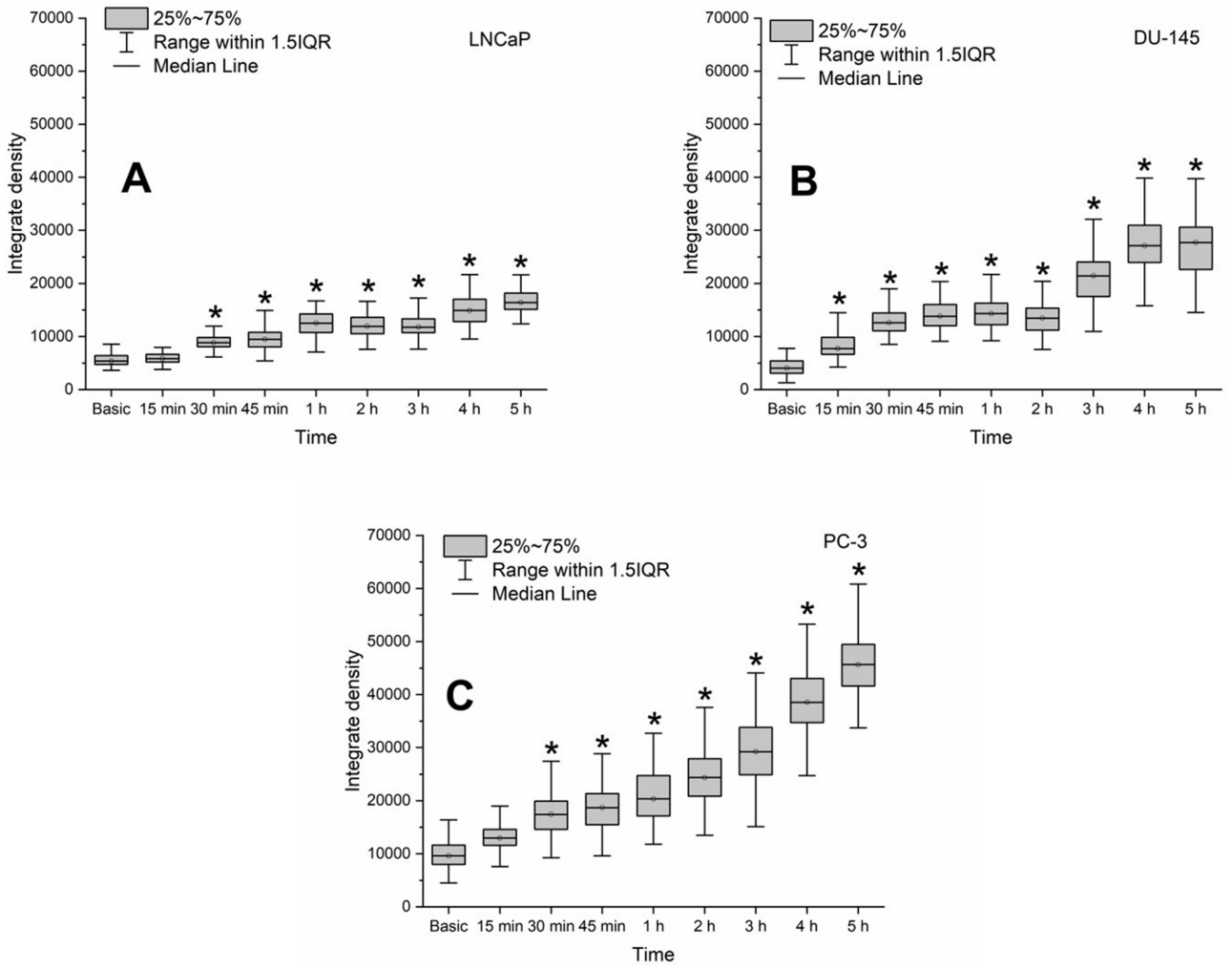

Figure 3 Zinc level in the prostate DU-145 (**A**), LNCaP (**B**) and PC-3 (**C**) cancer cell lines during their incubation with dextran-graft-polyacrylamide/ZnO nanoparticles (D-PAA/ZnO NPs) for 5 h (median, 25%-75%; Kruskal–Wallis test: *p < 0.05). Basic fluorescence is the fluorescence of cells without DPAA/ZnO NPs treatment. Staining with 30 μM TSQ for 30 min.

A three-fold elevation of the basal zinc level in LNCaP cells was detected. This parameter was 5.6-fold higher for DU-145 cells and 4.7-fold higher for PC-3 cells following 5 h of incubation with D-PAA/ZnO NPs. These were the maximum zinc levels for prostate cancer cells of low (LNCaP) and intermediate malignancy (DU-145). No maximum for zinc accumulation was found for high-malignancy prostate cancer cells (PC-3). Thus, they continued to absorb zinc from the incubation solution even after 5 h. Prostate cancer cells have an abnormal protein expression of the ZIP and ZnT family, which are responsible for zinc influx and efflux.[34,35] ZIP1 downregulation in PC-3 prevents the maintenance of normal zinc levels in cells, which explains high malignancy and metastatic potential.[36] The PC-3 cell line developed resistance to high zinc levels or zinc anticancer therapy via KRAS NF-κB-mediated pathways and changes in the expression of zinc transporters.[37] Thus, the D-PAA/ZnO nanosystem can overcome such cell defense systems and effectively increase the intracellular zinc level.

Importantly, malignant transformation of breast cells is accompanied by an increase in the zinc concentration, which is normally low.[38] Our findings indicate that the intracellular zinc accumulation correlates with the malignancy of breast cancer cell lines (Figure 4).

A statistically significant increase in the zinc amount was detected in MCF-7 cells after 15 min, MCF-7 Dox after 30 min, and MDA-MB-231 after 2 h of incubation, respectively. The maximum intracellular zinc level was registered after 4 h of incubation with D-PAA/ZnO NPs for all breast cancer cell lines (Supplementary Figures S7–S9).

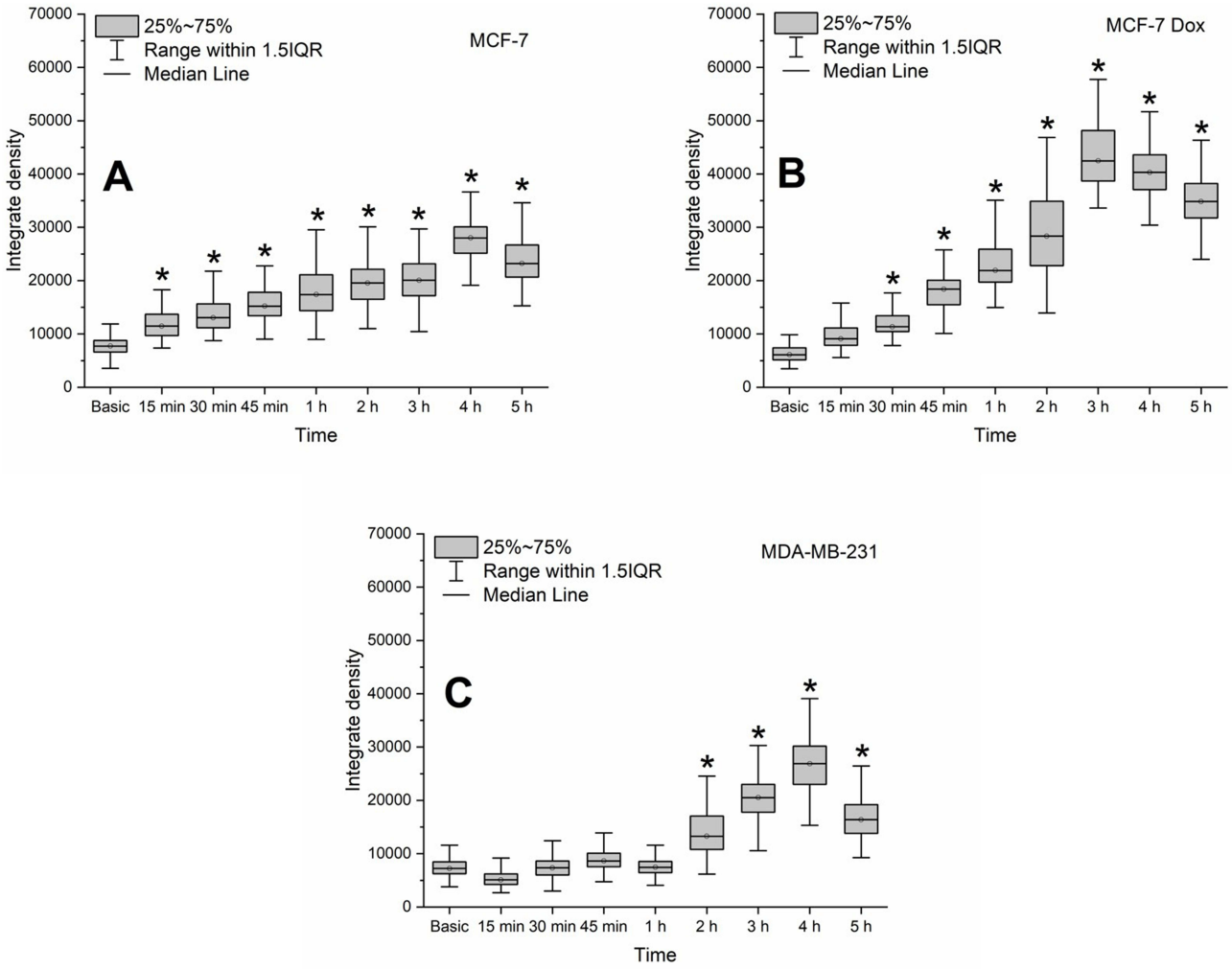

Figure 4 Zinc level in the MCF-7 (**A**) MCF-7 Dox (**B**) and MDA-MB-231 (**C**) breast cancer cell lines during their incubation with dextran-graft-polyacrylamide/ZnO nanoparticles (D-PAA/ZnO NPs) for 5 h (median, 25–75%; Kruskal–Wallis test: *p < 0.05). Basic fluorescence is the fluorescence of cells without D-PAA/ZnO NPs treatment. Staining with 30 μM TSQ for 30 min.

Accumulation of zinc ions in breast tumor tissues is associated with overexpression of Zn-transport proteins. Of note, upregulation of ZIP-family zinc transporters was found in breast cancer cells.[39] Metallothioneins and ZnT-family transporters play an important role in tumorigenesis of breast cancer. Mammalian metallothioneins are polypeptides of 61–68 amino acids. They have high cysteine content (30%) to bind to heavy metals including zinc and copper. ZnT-family proteins are zinc efflux transporters (ZnT1) or that pumping zinc into organelles. They were found to be upregulated in MDA-MB-231 cells.[40,41] Thus, in breast cancer cells zinc influx prevails over the zinc efflux. The decrease in zinc concentration was mediated by the activation of binding and Zn^{2+} efflux.

Intracellular zinc was quantified (Figure 5). Importantly, intracellular zinc levels correlated with the degree of malignancy of prostate and breast cancer cells. There is experimental evidence that zinc concentrations are diminished in prostate cancer cells during malignant transformation. Additionally, the zinc concentration in LNCaP cells is higher than in PC-3.[42,43]

Our findings reflecting intracellular zinc concentrations were consistent with the data of fluorescence microscopy. Excessive zinc accumulation was found in LNCaP and PC-3 prostate cancer cells after 24 h of incubation with D-PAA/ZnO NPs. A particularly dramatic 71.8-fold increase was found for PC-3 cells. In breast cancer cell lines, the amount of zinc corresponded to the level of cell malignancy.

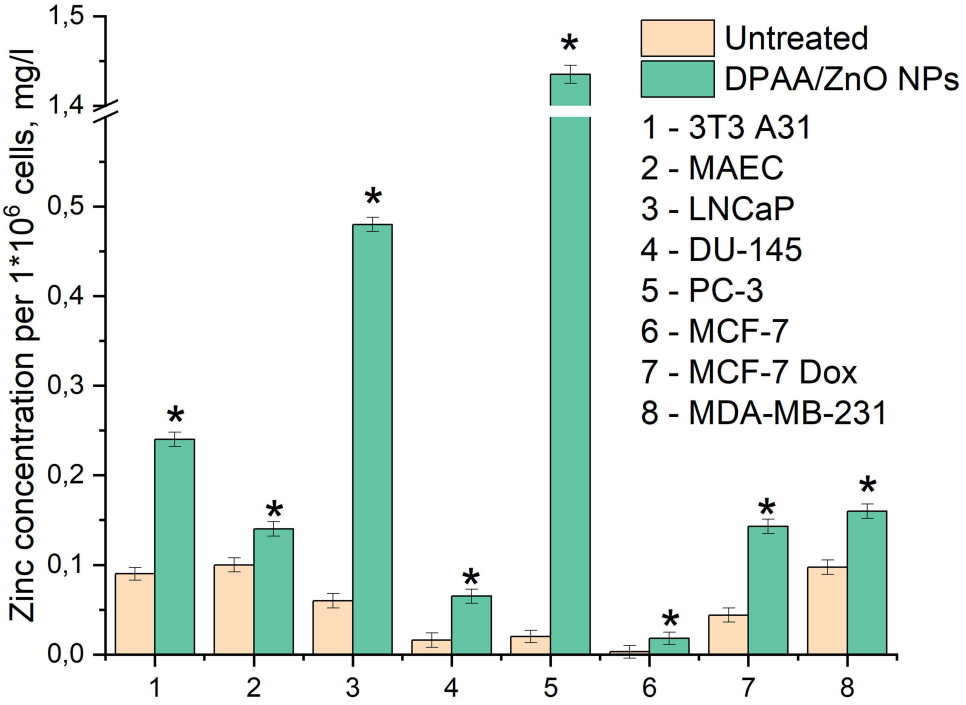

Figure 5 Zinc level in the prostate (LNCaP, DU-145, PC-3), breast cancer (MDA-MB-231, MCF-7 and MCF-7 Dox) and non-malignant (3T3 A31, MAEC) cell lines during their incubation with dextran-graft-polyacrylamide/ZnO nanoparticles (D-PAA/ZnO NPs) for 24 h (M±SD; ANOVA Scheffe test: *p < 0.05 compared to the untreated cells).

Thus, D-PAA/ZnO NPs nanosystems were internalized by prostate, breast cancer cells and non-malignant cells via endocytosis. The rate of absorption was dependent on the level of cell metabolism or the degree of their malignancy. ZnO NPs dissociation and release of Zn^{2+} into cytosol occurs in 2–3 hours. These processes were similar for cancerous and non-cancerous cells. High cytotoxicity to cancer cells reported earlier could be attributed to elevated intracellular Zn^{2+}.

It has been widely accepted that one of the ZnO NPs cytotoxicity mechanisms is ROS generation. ROS-generating effects could be attributed to the semiconducting properties of NPs and the presence of oxygen vacancy defects. A compelling body of evidence indicates that elevated ROS concentrations are observed in cells exposed to ZnO NPs.[44–47] Notably, ROS generation was independent of light irradiation.[48]

In the current study, we detected elevation of ROS levels by 26% and 40% in non-malignant 3T3 A31 cells and MAEC respectively, following exposure to the nanocomplex. A significant increase in ROS level was detected in prostate cancer cells after 24 h of incubation with D-PAA/ZnO NPs (Figure 6).

A 7.1-fold and 7.4-fold increase of ROS level was registered in LNCaP and DU-145 cells, respectively. This parameter was 4.4-fold higher in PC-3 cells. Changes in ROS levels were found to be prostate cancer cell lines malignancy-dependent. Elevation of intracellular ROS levels was revealed for breast cancer MCF-7, MCF-7 Dox and MDA-MB-231 cell lines to be 2.6-, 3-, and 3.2-fold, respectively. Thus, ROS upregulation was detected in all cells. Nevertheless, for non-malignant cells, the difference between the initial ROS level was insignificant. Accumulation of ZnO NPs and ROS overgeneration mediate cytotoxicity of the nanocomplex. A change in the shape of non-malignant cells to the spherical one was previously detected, but without visual signs of apoptosis. In the cancer cell lines, proapoptotic proteins were upregulated, and the cellular morphology showed alterations characteristic of apoptosis.[20]

Annexin V-FITC staining was used to detect lipid scrambling in 3T3 A31 fibroblasts and MAEC. As demonstrated in Figure 7, the cells exposed to D-PAA/ZnONPs nanocomplex did not have abnormal values of annexin V-positive PS-expressing cells indicating no cytotoxicity of the nanocomplex used.

The combined staining with annexin V-FITC and 7-AAD is a generally accepted approach that provides the opportunity to distinguish viable, early apoptotic, late apoptotic/necrotic and dead necrotic cells. As shown in

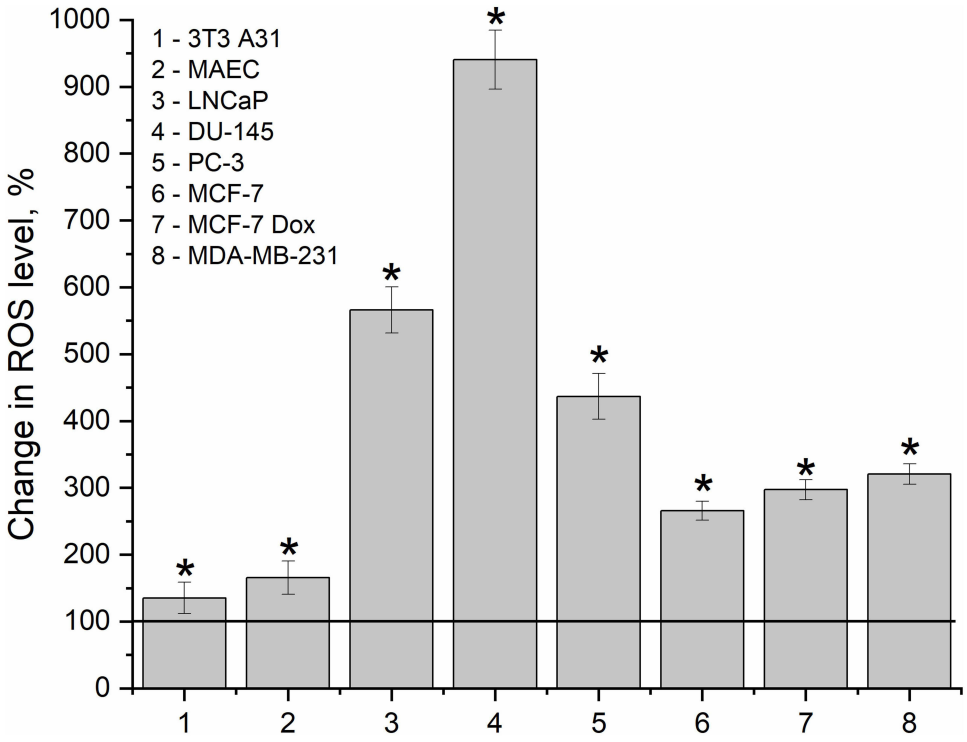

Figure 6 ROS levels in the prostate (LNCaP, DU-145, PC-3), breast cancer (MDA-MB-231, MCF-7 and MCF-7 Dox) and non-malignant (3T3 A31, MAEC) cell lines during their incubation with dextran-graft-polyacrylamide/ZnO nanoparticles (D-PAA/ZnO NPs) for 24 h. The difference in ROS levels was calculated relatively to D-PAA/ZnO NPs-untreated cells. The baseline level of ROS was taken as 100% (M±SD, Kruskal–Wallis test:*$p < 0.05$ compared to untreated cells).

Figure 8, exposure to D-PAA/ZnO NPs nanocomplex noticeably reduces the viability of DU-145 and LNCaP prostate cancer cell lines promoting cell death.

Notably, the similar cytotoxic effects were demonstrated for breast cancer cell lines (Figure 9). However, they were less pronounced.

To detect the toxicity of D-PAA/ZnO NPs nanocomplex, we analyzed its impact on phospholipid scrambling in normal murine 3T3 A31 fibroblasts and MAEC. PS externalization is commonly observed in apoptosis, necroptosis, as well as in stressed and senescent cells.[49–52] Importantly, PS-expressing cells are detected by macrophages, since PS located in the outer leaflet of cell membrane acts as an "eat-me" signal promoting efferocytosis.[53] Thus, evaluation of PS externalization covers a wide range of cytotoxicological effects compared to specific apoptosis markers alone. Our findings suggest that D-PAA/ZnO NPs nanocomplex does not promote PS externalization indicating lack of toxicity against normal cells at the concentration used. To assess therapeutic potential of D-PAA/ZnO NPs nanocomplex as an anti-cancer drug, we evaluated its cytotoxicity in vitro using several prostate and breast cancer cell lines. The present study revealed that D-PAA/ZnO NPs nanocomplex efficiently promoted cell death of tumor cells without showing cytotoxicity towards normal cells making it a promising anti-cancer agent. Further in-death evaluation of its toxicity and effectiveness should be encouraged.

Neoplastic transformation of cells is accompanied by metabolic reprogramming. Changes in cellular metabolism are necessary to meet the high requirements for ATP and biomolecules. As a result, cancer cells consume much more glucose than non-malignant cells.[54]

No statistically significant changes in glucose consumption by non-malignant 3T3 A31 and MAEC cells were found after 24 h of incubation with D-PAA/ZnO NPs (Figure 10A).

Glucose consumption in prostate cancer DU-145 and PC-3 was reduced by 15–20%. Less malignant LNCaP prostate cancer cells did not alter glucose metabolism following exposure to D-PAA/ZnO NPs. MDA-MB-231 breast cancer cells were the most sensitive to D-PAA/ZnO NPs. Glucose uptake was found to be reduced almost twice. No changes in

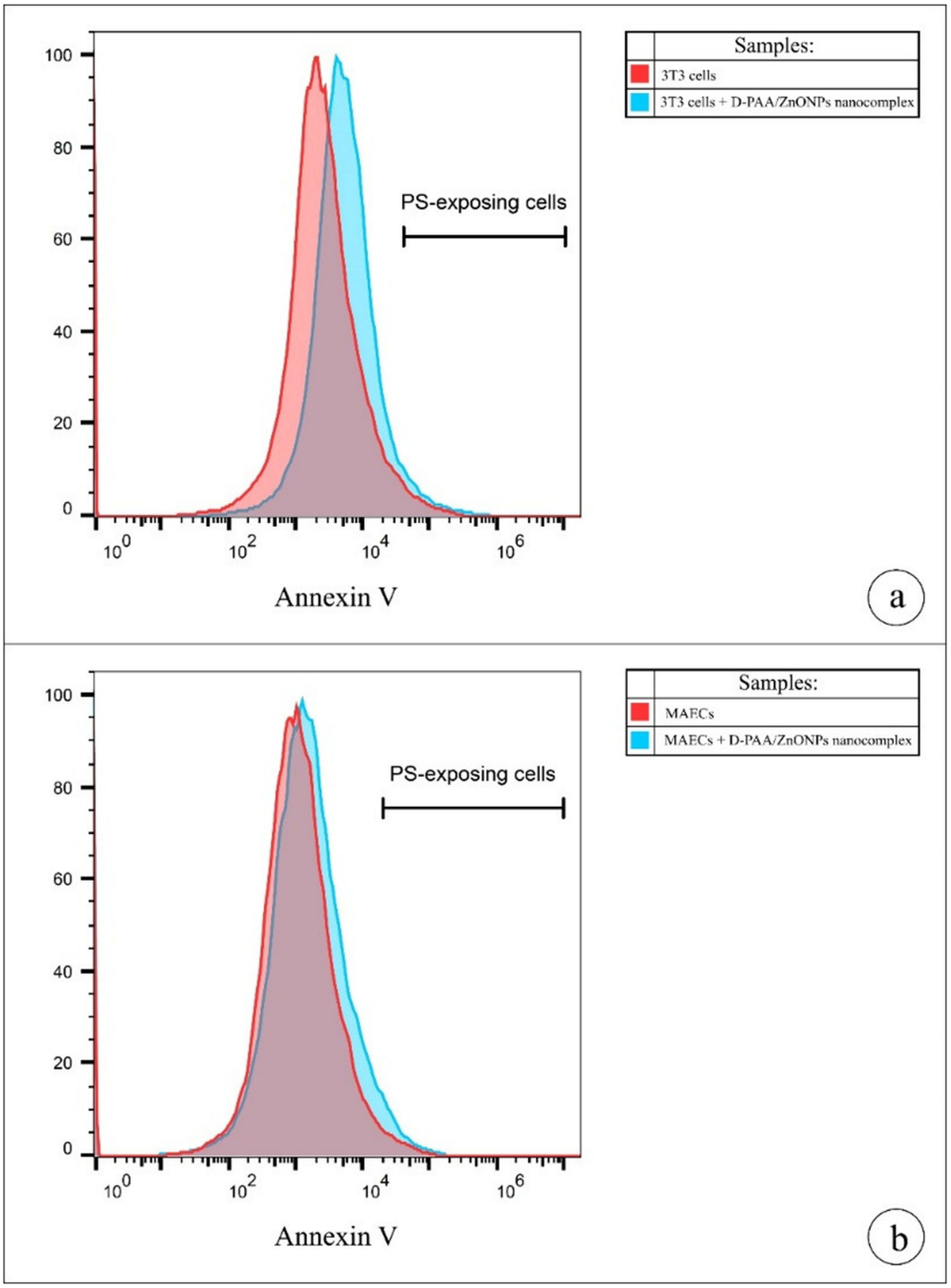

Figure 7 D-PAA/ZnO NPs nanocomplex does not induce phosphatidylserine (PS) externalization in murine 3T3 fibroblasts (**a**) and mouse aortic endothelial cells (**b**). Representative histograms demonstrate the population of PS-displaying cells. Data were statistically processed using Mann–Whitney *U*-test (n = 3). No statistically significant changes between the percentage of PS-exposing cells were found ($p > 0.05$).

glucose consumption were detected for MCF-7 and MCF-7 Dox breast cancer cell lines. Thus, highly malignant cells were associated with reduced glucose uptake in the presence of D-PAA/ZnO NPs.

Glucose metabolism is rewired in cancer cells. Hypoxia promotes the lactate production, which correlates with tumor aggressiveness, metastatic potential, and invasion.[55,56] Reduced lactate production is one of the strategies for decreasing the malignancy level of tumors.[57] Lactate production by triple-native breast cancer cells provides a basis for prognostic models.[58] Diminishment of lactate concentration in the incubation medium by 20–30% was found for all cancer cell lines following treatment with D-PAA/ZnO NPs (Figure 10B). Lactate production was not affected (3T3 A31) or reduced by

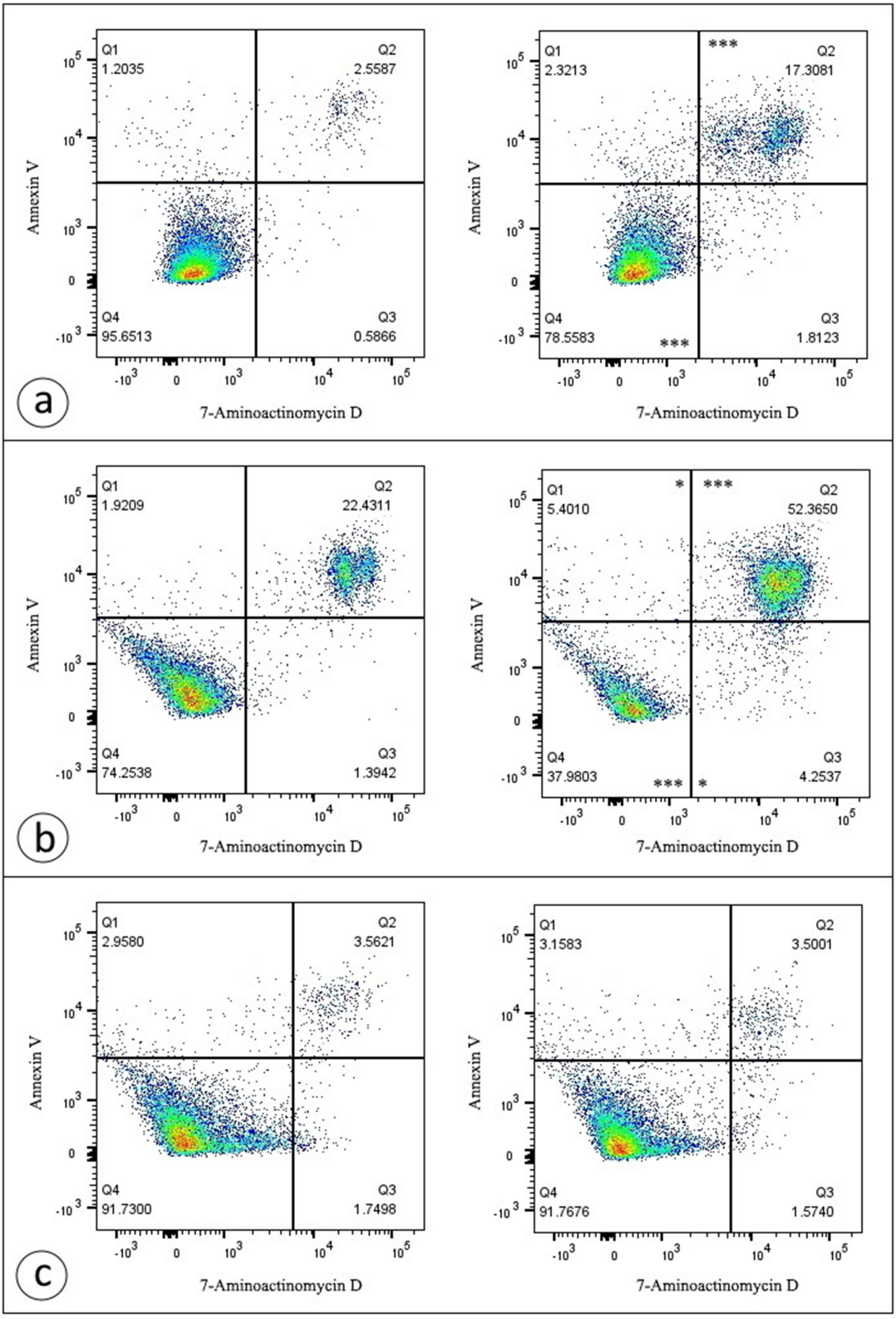

Figure 8 D-PAA/ZnONPs nanocomplex triggers cell death in prostate cancer cell lines. Representative dotplots are provided for DU-145 (**a**), LNCaP (**b**), and PC-3 (**c**) cells. Exposure to D-PAA/ZnO NPs nanocomplex increased the percentage of late apoptotic/necrotic cells for DU-145 cell line, as well as early apoptotic, late apoptotic/necrotic and dead necrotic cells for LNCaP cell line. Data were statistically processed using Mann–Whitney *U*-test (n = 3).
Notes: *p < 0.05; ***p < 0.001 compared with the control samples.

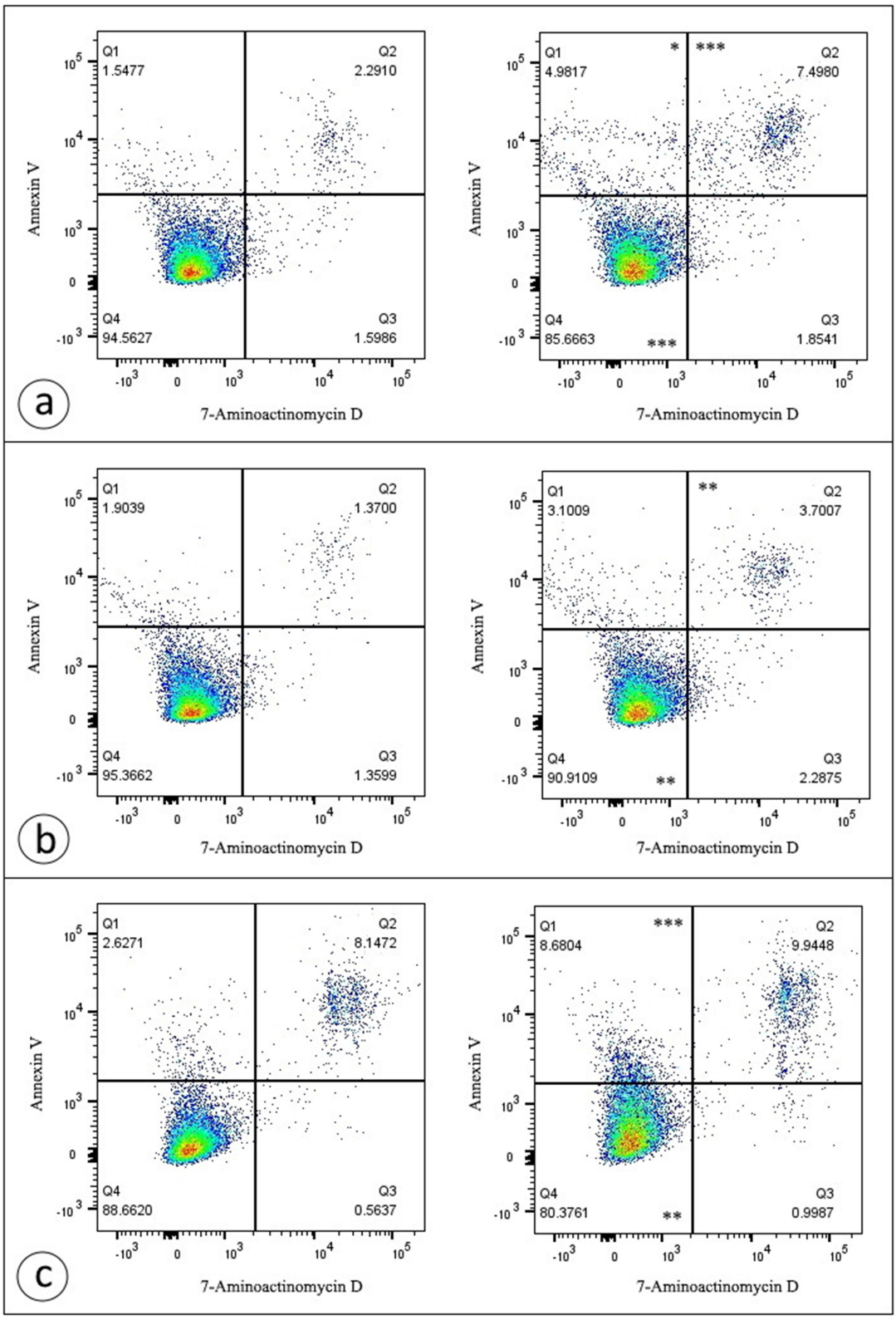

Figure 9 D-PAA/ZnO NPs nanocomplex promotes cell death in breast cancer cell lines to a lesser extent than in prostate cancer cell lines. Representative dotplots are demonstrated for MCF-7 (**a**), MCF-7Dox (**b**), and MDA-MB-231 (**c**) cells. Treatment of cells with D-PAA/ZnONPs nanocomplex enhanced the percentage of early apoptotic, late apoptotic/necrotic cells for MCF-7 cell line, as well as late apoptotic/necrotic cells for MCF-7Dox cell line and early apoptotic cells for MDA-MB-231 cells. Data were statistically processed using Mann–Whitney *U*-test (n = 3).

Notes: *p < 0.05; **p < 0.01; ***p < 0.001 compared with the control samples.

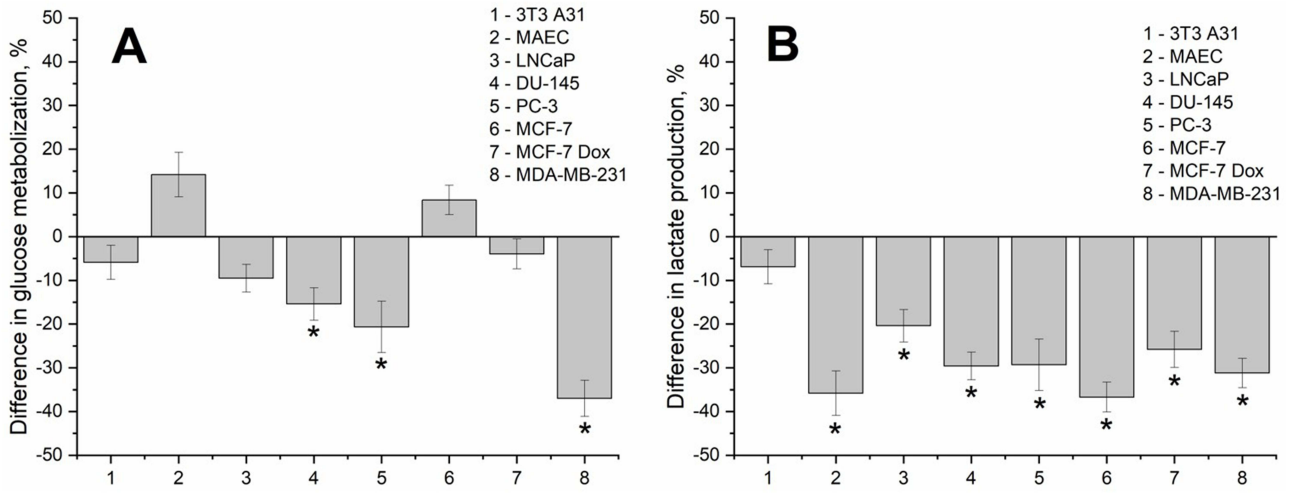

Figure 10 Glucose uptake (**A**) and lactate production (**B**) in the prostate (LNCaP, DU-145, PC-3), breast cancer (MDA-MB-231, MCF-7, MCF-7 Dox) and non-malignant (3T3 A31, MAEC) cell lines after incubation with dextran-graft-polyacrylamide/ZnO nanoparticles (D-PAA/ZnO NPs) for 24 h (M±SD, *p < 0.05 compared to untreated cells).

30% (MAEC) for non-malignant cells. Initial lactate production by cancer cell lines was 30–40% higher than for the non-malignant ones.

Other studies have shown the impact of ZnO NPs on the lactate production of other cancer cells in vitro and in vivo.[59,60]

Our findings indicate that D-PAA/ZnO NPs reduce glucose consumption and lactate production by cancer cells. The rate of carbohydrate metabolism in cancer cells was reduced by D-PAA/ZnO NPs.

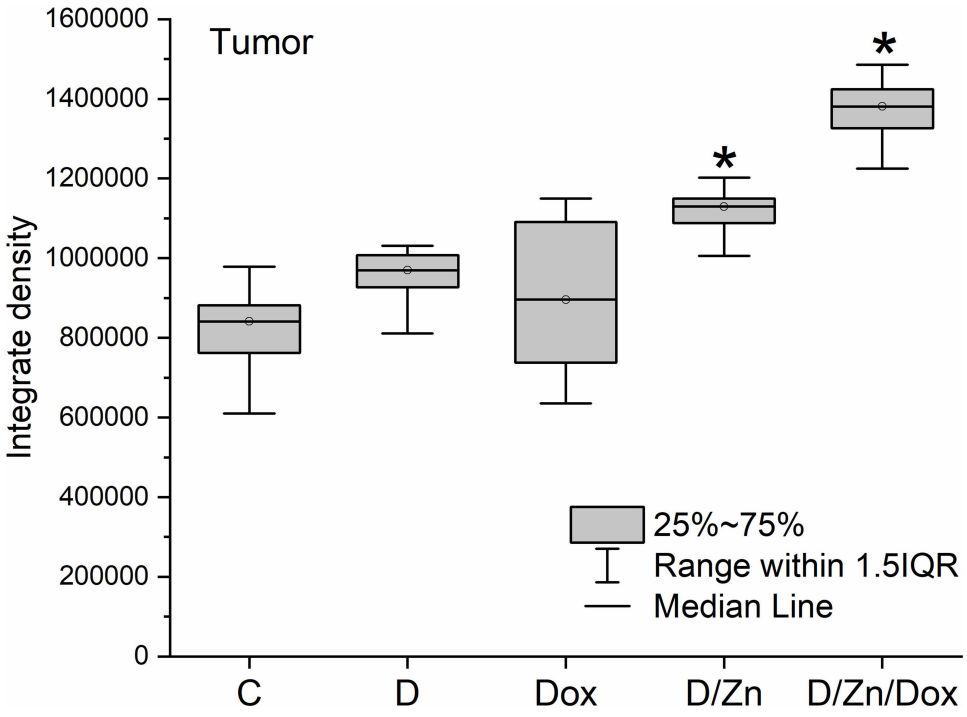

Figure 11 Relative zinc content in tissues of Walker-256 carcinosarcoma after intravenous injection of saline (C), D-PAA (D), doxorubicin (Dox), D-PAA/ZnO NPs (D/Zn), D-PAA/ZnO NPs/Dox (D/Zn/Dox) for 5 days. Staining with 30 μM TSQ in PBS for 30 min; (Median, 25%-75%, *p < 0.05). The volume of a single injection was 0.5 mL. Doxorubicin dosage was 1.5 mg/kg of rat weight, ZnO NPs was 200 μMol/kg.

Zinc and zinc-containing nanomaterials have a high affinity for proteins.[9,61] ZnO NPs interact with blood plasma and form a protein corona.[62–64] In this state, they are transported to tissues and organs. ZnO NPs accumulate in various tissues and can disrupt their functions.[65]

In the current study, the light transmittance (530 nm) of 3 mM D-PAA/ZnO NPs aqueous solutions was about 40% (Supplementary Figure S10). The solution of bovine serum albumin (40 mg/mL) was almost transparent, whereas the light transmittance was 95%. A decrease in the light transmittance to 40% was detected after adding D-PAA/ZnO NPs to the albumin solution, but the return to the original state of the transmittance (95%) was registered already following 30 min. Similar changes were detected when blood serum was incubated with D-PAA/ZnO NPs.

Thus, ZnO NPs due to their high affinity to proteins are at least partially transferred by blood plasma proteins. Interaction occurs quite rapidly. The solutions are stable for 24 hours.

The advantages of the therapeutic application of nanoparticles include their small size, high penetration into tissues and the ability to overcome various barriers. This makes it possible to create anticancer drug delivery and diagnostics systems based on ZnO NPs.[66–68] A number of studies have shown that ZnO NPs are accumulated in the liver and kidneys.[69–71] Excessive ZnO NPs promote organ dysfunction in an oxidative stress dependent fashion.[72] At the same

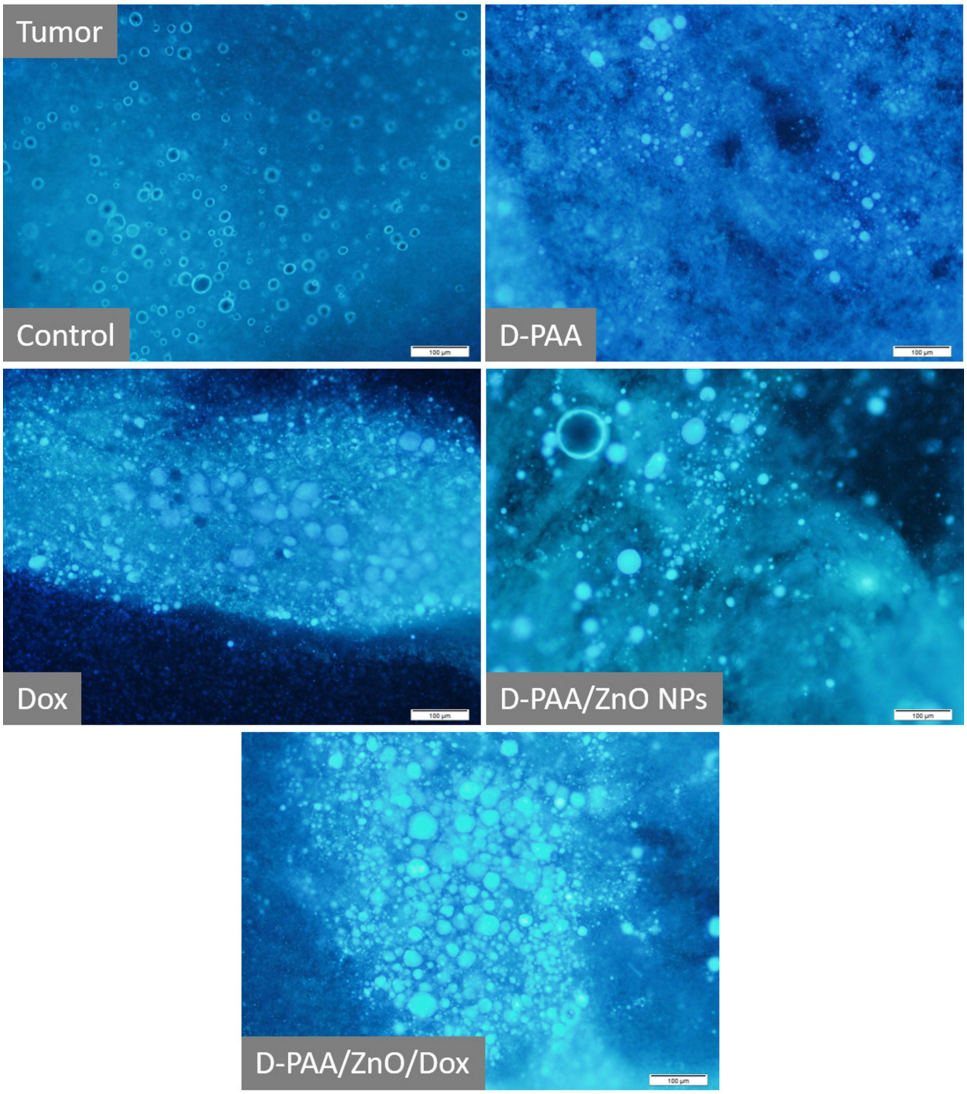

Figure 12 Zinc accumulation in Walker-256 carcinosarcoma tissues after intravenous injection of saline (Control), D-PAA, doxorubicin (Dox), D-PAA/ZnO NPs and D-PAA/ZnO NPs/Dox for 5 days. Staining with 30 μM TSQ for 30 min. An increase in the zinc level in the cells was found after treatment with D-PAA/ZnO NPs and D-PAA/ZnO NPs/Dox (Scale bar is 100 μm).

time, ZnO NPs have protective effects on tissues in relation to highly toxic anticancer drugs such as doxorubicin.[73,74] In this study, we assessed hepatic, renal, splenic and tumor accumulation of D-PAA/ZnO NPs following intravenous injection of D-PAA/ZnO NPs. The doxorubicin was used as a reference anticancer drug.

Baseline of zinc content in the tumor was not modified as a result of intravenous injection of D-PAA and Dox. No changes in zinc content were detected in Walker-256 carcinosarcoma tissues after treatment with the polymer or doxorubicin (Figure 11).

Zinc content in tumors increased by 25% following D-PAA/ZnO NPs and 39% with D-PAA/ZnO NPs/Dox treatment. Thus, doxorubicin contributed to increased permeability and greater zinc accumulation in tumor tissues. An increase in zinc levels for tumor cells were found in animals exposed to D-PAA/ZnO NPs and D-PAA/ZnO NPs/Dox (Figure 12). This indicated the delivery of nanosystems to tumor cells.

The growth of Walker-256 carcinosarcoma tumors was slowed down compared to controls after treatment with D-PAA/ZnO NPs (Figure 13). This was most likely mediated by the uptake and accumulation of D-PAA/ZnO NPs in the cancer cells. Consistently, other studies have reported positive therapeutic effects of ZnO NPs in hepatocellular carcinoma and 39 murine breast cancer models in vivo.[75,76]

The tumor volume was 65 times lower than the control one when treated with doxorubicin 1.5 mg/kg for 5 days. These values were almost unaffected when using D-PAA/ZnO NPs/Dox. Thus, no influence of D-PAA/ZnO NPs on the

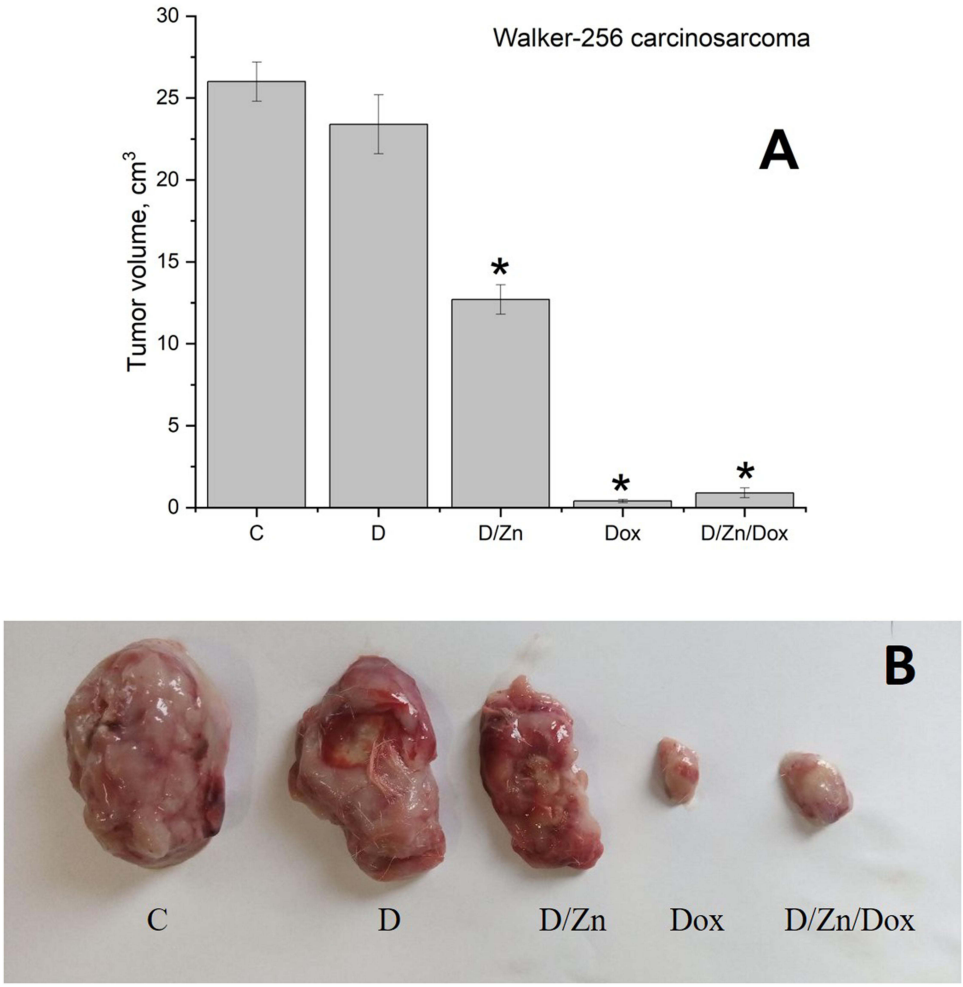

Figure 13 Tumor volume (**A**) and a visual comparison (**B**) of Walker-256 carcinosarcoma following intravenous injection of saline (C), D-PAA (D), doxorubicin (Dox), D-PAA/ZnO NPs (D/Zn), D-PAA/ZnO NPs/Dox (D/Zn/Dox) for 5 days. Staining with 30 μM TSQ in PBS for 30 min (M±SD, *p<0.05). The volume of a single injection was 0.5 mL. Doxorubicin dosage was 1.5 mg/kg of rat weight, ZnO NPs was 200 μMol/kg.

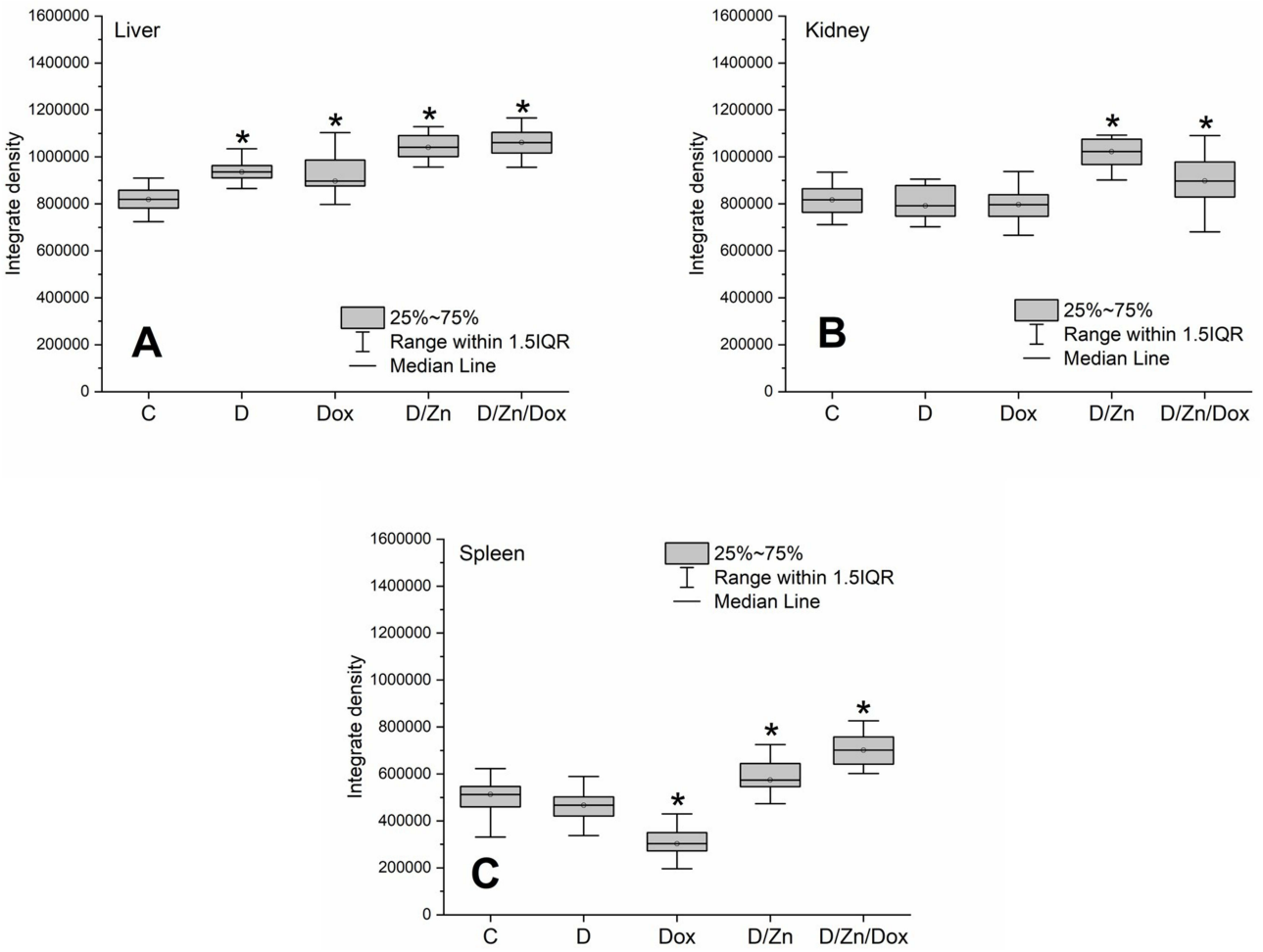

Figure 14 Relative zinc content in tissues of liver (**A**), kidney (**B**) and spleen (**C**) after intravenous injection of saline (C), D-PAA (D), doxorubicin (Dox), D-PAA/ZnO NPs (D/Zn), D-PAA/ZnO NPs/Dox (D/Zn/Dox) for 5 days. Staining with 30 μM TSQ in PBS for 30 min (Median, 25%-75%, *p<0.05). The volume of a single injection was 0.5 mL. Doxorubicin dosage was 1.5 mg/kg of rat weight, ZnO NPs was 200 μMol/kg.

antitumor efficacy of Dox in vivo was found. This proves the possibility of combined administration of D-PAA/ZnO NPs and Dox for the anti-cancer therapy.

Elevated zinc content was observed in hepatic tissue following intravenous injection of D-PAA, Dox, D-PAA/ZnO NPs and D-PAA/ZnO NPs/Dox (Figure 14A, Supplementary Figure S11). The liver plays a crucial role in zinc metabolism.[77,78] It has been hypothesized that metabolized Dox and D-PAA might increase hepatic zinc content. The zinc level was elevated by no more than 10–12%. Higher zinc level in hepatic tissues by 20% was found in case of exposure to D-PAA/ZnO NPs and D-PAA/ZnO NPs/Dox.

A 20% increase in zinc levels was found in the renal tissue following treatment with D-PAA/ZnO NPs (Figure 14B, Supplementary Figure S12). This parameter was 10% higher in case of D-PAA/ZnO NPs/Dox treatment. Zinc content was reduced by 40% in the spleen as a result of intravenous injection of Dox (1.5 mg/kg) for 5 days. Perhaps this was due to the drug-induced splenic toxicity which contributed to the leakage of zinc into the bloodstream. An increase in zinc levels by 10% and 27% in the spleen was registered after the D-PAA/ZnO NPs and D-PAA/ZnO NPs/Dox treatments, respectively (Figure 14C, Supplementary Figure S13). A mild accumulation of zinc in organs can reduce the toxic effects and tissue damage during doxorubicin anticancer therapy.[73,74]

Basophilic spherical cells with large nuclei were found in tumor tissue of control animals. Approximately 20% of the cells had signs of apoptosis or necrosis such as eosinophilic cytoplasm, pyknotic nuclei or lack of nuclei. The tissue was permeated with connective tissue fibers with interspersed adipose tissue (Figure 15).

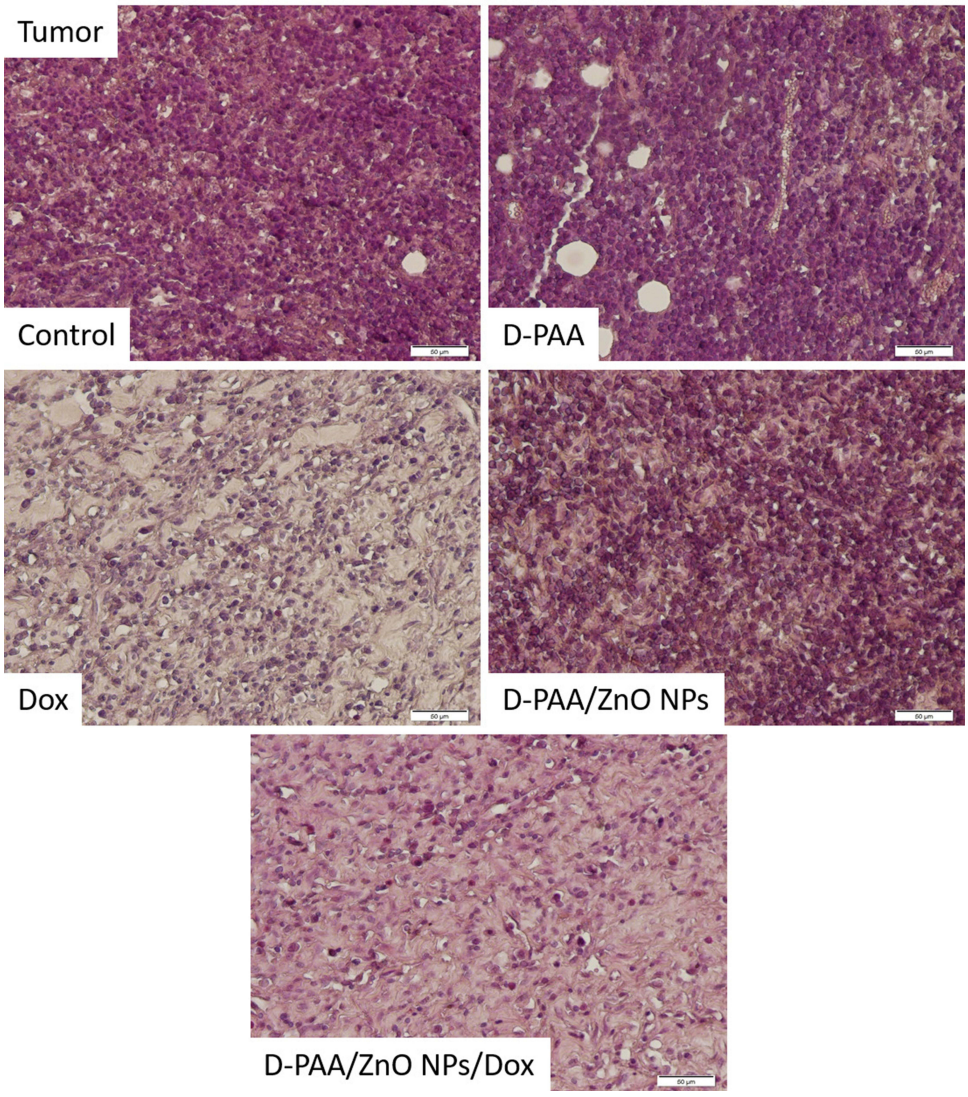

Figure 15 Histopathologic changes in Walker-256 carcinosarcoma tissues after intravenous injection of saline (Control), D-PAA, doxorubicin (Dox), D-PAA/ZnO NPs and D-PAA/ZnO NPs/Dox for 5 days. Hematoxylin and eosin staining. For doxorubicin and D-PAA/ZnO NPs/Dox, tissue cellularity was greatly reduced. (Scale bar is 50 μm).

These tissue characteristics were found when animals were treated with D-PAA. However, the relative number of cells with signs of apoptosis was increased. This indicated the D-PAA interaction with the tumor and cancer cells, but the mechanisms of apoptosis induction by the polymer nanocarrier in vivo need to be elucidated (Figure 15). In vitro studies on non-malignant and cancerous cells revealed no changes in cellular survival or apoptosis following treatment with D-PAA.[20] No significant changes compared to the control samples and D-PAA in the morphology of tumor tissues and cells were found after D-PAA/ZnO NPs treatment of animals. A large number of apoptotic bodies, pyknotic nuclei, and cells without nuclei were identified. The cell number in the tumor tissue was significantly reduced after treating the animals with doxorubicin (Figure 15). The vast majority of cells had signs of apoptosis or necrosis. The combined application of D-PAA/ZnO NPs and Dox enhanced antitumor effects. A high proportion of irregularly shaped cells, apoptotic bodies and cells with pyknotic nuclei were identified (Figure 15).

A large number of Kupffer cells were identified in the hepatic tissue of the control group of animals. Blood stasis in the central veins and cells with signs of apoptosis were registered (Figure 16). Changes in hepatic tissue similar to the control group were found after treatment of animals with D-PAA. The number of Kupffer cells was reduced compared

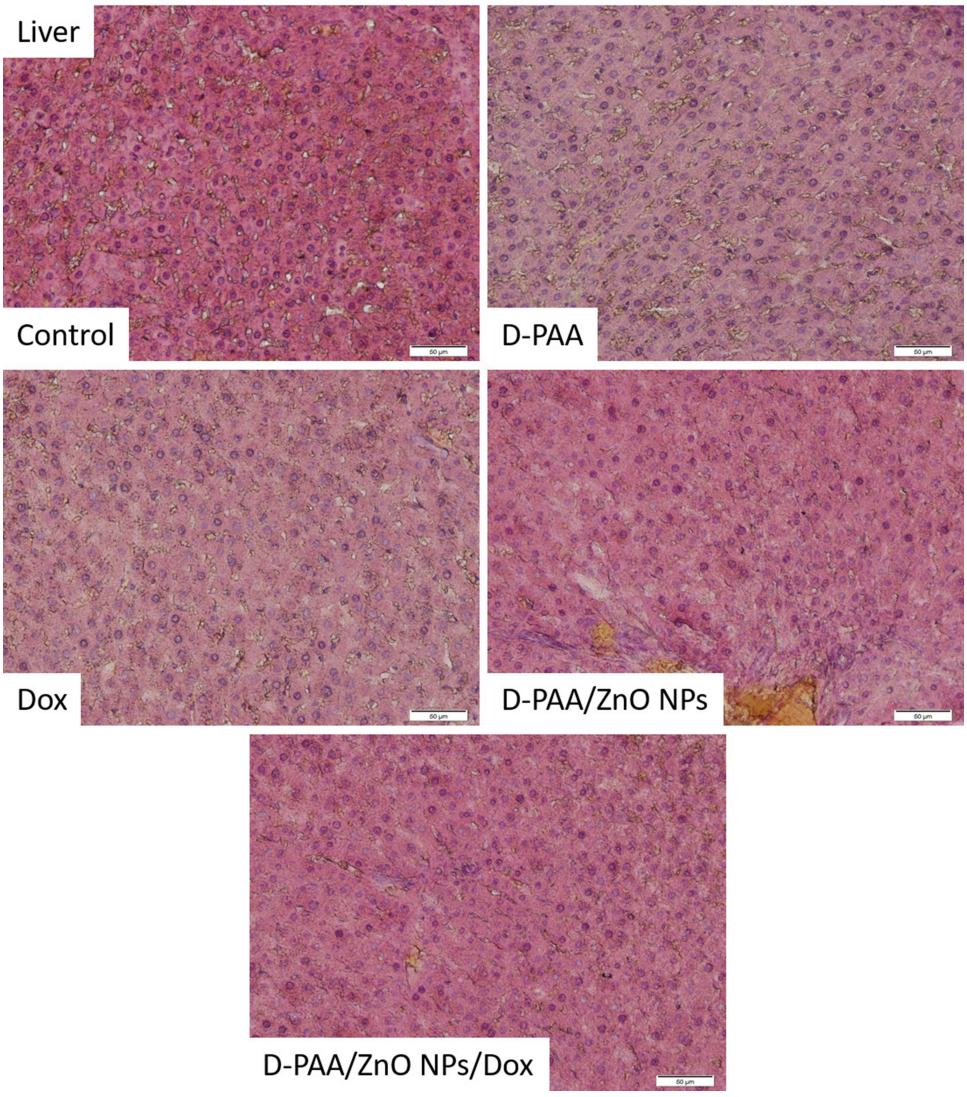

Figure 16 Histopathologic changes in liver after intravenous injection of saline (Control), D-PAA, doxorubicin (Dox), D-PAA/ZnO NPs and D-PAA/ZnO NPs/Dox for 5 days. No significant pathological changes were identified in the liver tissues for all animal groups. Individual apoptotic cells and a significant number of Kupffer cells were found. (Scale bar is 50 μm).

with the control samples. Accumulation of inflammatory infiltrate was revealed around the central veins (Figure 16). Eosinophilic cytosolic inclusions were found in some hepatocytes. No significant morphological changes were found in liver tissues compared with the controls following treatment with D-PAA/ZnO NPs. However, no cells with signs of apoptosis or necrosis were identified (Figure 16). Thus, ZnO NPs were hepatoprotective and prevented the development of some liver dysfunctions in cancer, which was demonstrated in other studies as well.[73,74] No significant pathological alterations were identified in the hepatic tissue after animal treatment with doxorubicin. Cells with karyomegaly and blood stasis were found in the central veins.

The number of cells with an karyomegaly, Kupffer cells, apoptotic and necrotic cells were found in hepatic tissue after the combined treatment of animals with D-PAA/ZnO NPs and Dox (Figure 16). Thus, the toxic effect of doxorubicin on the liver was diminished by D-PAA/ZnO NPs and the negative consequences of the tumor process were also reduced.

Single hyperplastic regeneration and loss of the border of tubulocytes were observed in the control group of animals. The renal tissue in animals of the control group was not pathologically altered (Figure 17). The renal tubular apparatus

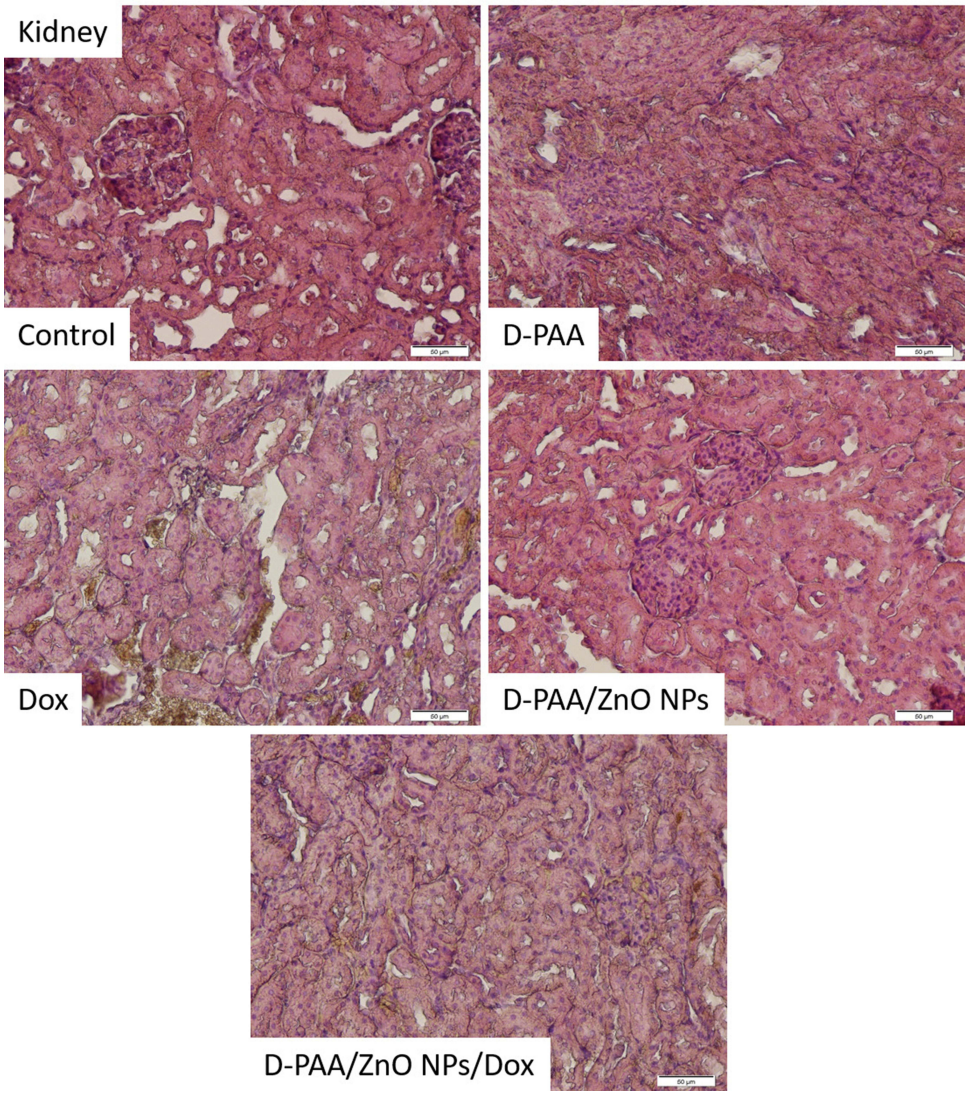

Figure 17 Histopathologic changes in the kidney after intravenous injection of saline (Control), D-PAA, doxorubicin (Dox), D-PAA/ZnO NPs and D-PAA/ZnO NPs/Dox for 5 days. (Scale bar is 50 μm).

was preserved, but the lumen of the nephron capsule was reduced and the shape of the glomeruli was changed to the irregular one after animal treatment with D-PAA (Figure 17). Morphological tissue changes indicate some nephrotoxicity of D-PAA. An increase in the lumen of the nephron capsule and isolated cases of loss of the border cells of the tubules were found after animal treatment with D-PAA/ZnO NPs (Figure 17). Necrosis of tubulocytes, loss of tubular cellular living, flattening of the tubular epithelium were identified when doxorubicin was used to treat cancer (Figure 17). The loss of tubulocyte borders, cells with pyknotic nuclei, blood stasis in capillaries and increased tubulo-intestinal cellularity were found after the combined treatment of animals with D-PAA/ZnO NPs and doxorubicin (Figure 17).

No pathological changes in splenic tissues were found in animals of the control group (Figure 18). Slight white pulp hypoplasia and well-developed red splenic pulp were observed in D-PAA-treated rats. The identified changes indicated weak inhibition of leukopoiesis. Solitary apoptotic cells were detected (Figure 18).

The white pulp and red pulp of the spleen were well developed after treatment of animals with D-PAA/ZnO NPs (Figure 18). Well-developed red pulp capillaries were found. Severe hypoplasia of the splenic white pulp was revealed after treatment with doxorubicin (Figure 18). The changes were typical for doxorubicin anticancer therapy. Slight hypoplasia of the white pulp was found following the D-PAA/ZnO NPs and Doxorubicin cancer treatment

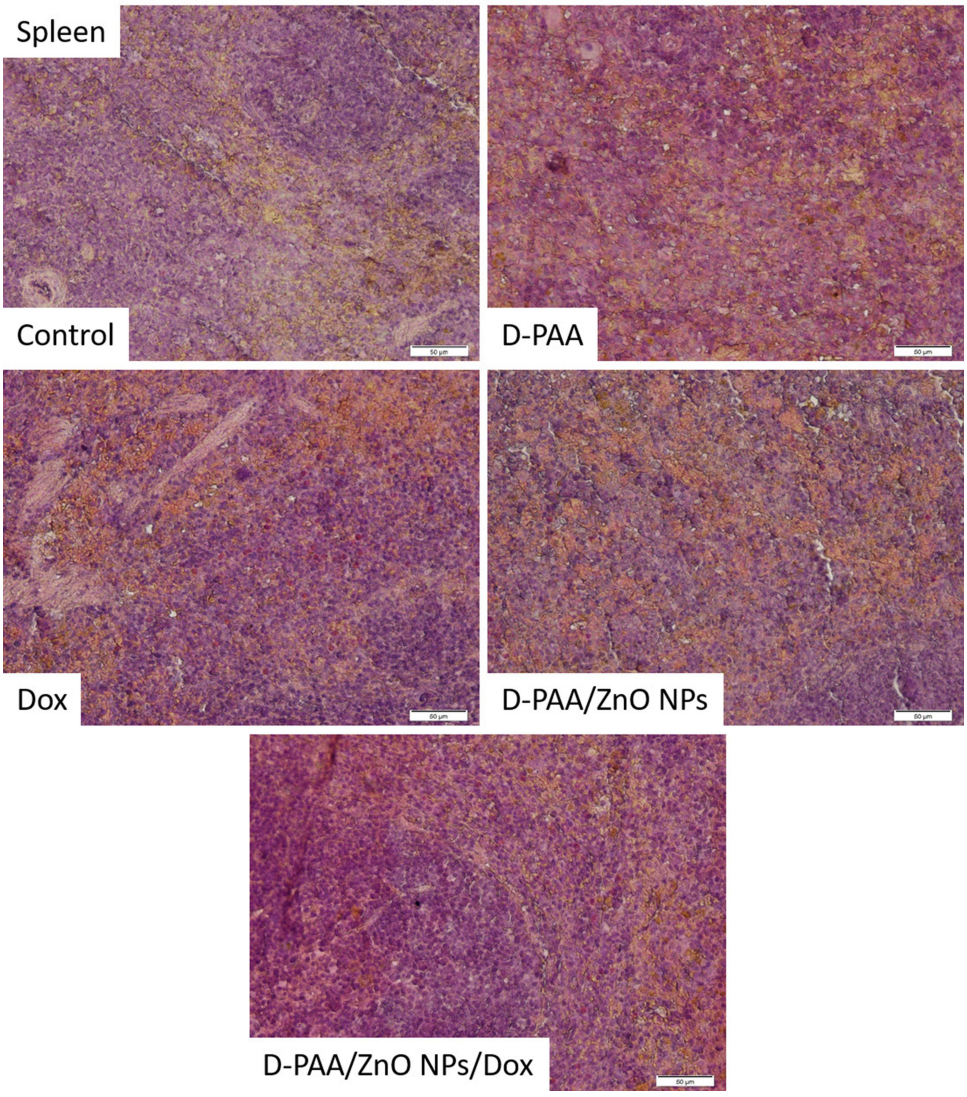

Figure 18 Histopathologic changes in spleen after intravenous injection of saline (Control), D-PAA, doxorubicin (Dox), D-PAA/ZnO NPs and D-PAA/ZnO NPs/Dox for 5 days. Severe hypoplasia of the splenic white pulp was found after treatment with doxorubicin, D-PAA/ZnO NPs and D-PAA/ZnO NPs/Dox. (Scale bar is 50 μm).

(Figure 18). Thus, the negative consequences of doxorubicin application for the spleen were diminished as a result of the combined treatment with D-PAA/ZnO NPs.

Conclusion

D-PAA/ZnO NPs nanosystems were internalized by prostate, breast cancer cells and non-malignant cells via endocytosis after 15–45 min of incubation, zinc release into cytosol occurs in 2–3 h. These processes were similar for cancerous and non-malignant cells. ROS upregulation was detected in all cells. Nevertheless, for non-malignant cells, the difference between the initial ROS level was insignificant. The rate of carbohydrate metabolism in cancer cells was reduced by D-PAA/ZnO NPs. D-PAA/ZnO NPs nanocomplex efficiently promoted cell death of tumor cells without showing cytotoxicity against non-malignant cells making it a promising anti-cancer agent. In vivo model study reveals that the volume of Walker-256 tumor carcinosarcoma was half as much than the control one when treated with D-PAA/ZnO NPs. No impact of D-PAA/ZnO NPs on the antitumor effectiveness of Dox in vivo was found. This proves the possibility of combined administration of D-PAA/ZnO NPs and Dox for the anticancer therapy. Thus, the D-PAA/ZnO NPs nanosystem inhibits cancer cells and has a weak effect on non-malignant ones. These properties were preserved in vivo models after treatment for up to 5 days. In addition, when co-treatment with doxorubicin, the

toxicity effects on the tumor were preserved. Thus, D-PAA/ZnO NPs nanosystems can potentially be used as anticancer agents both individually and in combination with doxorubicin. In future studies, we plan to improve the targeting of the D-PAA/ZnO NPs by modifying the copolymer carrier as well as evaluate the effectiveness of combined treatment with ultrasound.

Data Sharing Statement

Data are within the article.

Acknowledgments

Catherine Foussat and Mélanie Legros from the characterization group of the Institut Charles Sadron (Strasbourg, France) for size exclusion chromatography characterization of the star-like polymer. Authors are grateful to brave defenders of Ukraine for the opportunity to finalize this publication.

Funding

This study was supported in part by the Ministry of the Education and Science of Ukraine, Project no. 0124U001177.

Disclosure

The authors report no conflicts of interest in this work.

References

1. Rasmussen JW, Martinez E, Louka P, Wingett DG. Zinc oxide nanoparticles for selective destruction of tumor cells and potential for drug delivery applications. *Expert Opin Drug Deliv*. 2010;7(9):1063–1077. doi:10.1517/17425247.2010.502560
2. Rabaan AA, Bukhamsin R, AlSaihati H, et al. Recent trends and developments in multifunctional nanoparticles for cancer theranostics. *Molecules*. 2022;27(24):8659. doi:10.3390/molecules27248659
3. Singh TA, Das J, Sil PC. Zinc oxide nanoparticles: a comprehensive review on its synthesis, anticancer and drug delivery applications as well as health risks. *Adv Colloid Interface Sci*. 2020;286:102317. doi:10.1016/j.cis.2020.102317
4. Bozym RA, Chimienti F, Giblin LJ, et al. Free zinc ions outside a narrow concentration range are toxic to a variety of cells in vitro. *Exp Biol Med*. 2010;235(6):741–750. doi:10.1258/ebm.2010.009258
5. Anderson NM, Simon MC. The tumor microenvironment. *Curr Biol*. 2020;30(16):R921–R925. doi:10.1016/j.cub.2020.06.081
6. Hassanian M, Aryapour H, Goudarzi A, Javan MB. Are zinc oxide nanoparticles safe? A structural study on human serum albumin using in vitro and in silico methods. *J Biomol Struct Dyn*. 2021;39(1):330–335. doi:10.1080/07391102.2019.1711189
7. Singh S. Zinc oxide nanoparticles impacts: cytotoxicity, genotoxicity, developmental toxicity, and neurotoxicity. *Toxicol Mech Methods*. 2019;29(4):300–311. doi:10.1080/15376516.2018.1553221
8. Choi SJ, Choy JH. Biokinetics of zinc oxide nanoparticles: toxicokinetics, biological fates, and protein interaction. *Int J Nanomed*. 2014;9(Suppl 2):261–269. doi:10.2147/IJN.S57920
9. Sudhakaran S, Athira S, Suresh Babu S, et al. Determination of the bioavailability of zinc oxide nanoparticles using ICP-AES and associated toxicity. *Colloids Surf B Biointerfaces*. 2020;188:110767. doi:10.1016/j.colsurfb.2019.110767
10. Srivastav AK, Dhiman N, Khan H, et al. Impact of surface-engineered ZnO nanoparticles on protein corona configuration and their interactions with biological system. *J Pharm Sci*. 2019;108(5):1872–1889. doi:10.1016/j.xphs.2018.12.021
11. Cui T, Yan Z, Qin H, et al. A sequential target-responsive nanocarrier with enhanced tumor penetration and neighboring effect in vivo. *Small*. 2019;15(42):e1903323. doi:10.1002/smll.201903323
12. Li X, Yu X, Dai D, et al. The altered glucose metabolism in tumor and a tumor acidic microenvironment associated with extracellular matrix metalloproteinase inducer and monocarboxylate transporters. *Oncotarget*. 2016;7(17):23141–23155. doi:10.18632/oncotarget.8153
13. Kennedy KM, Dewhirst MW. Tumor metabolism of lactate: the influence and therapeutic potential for MCT and CD147 regulation. *Future Oncol*. 2010;6(1):127–148. doi:10.2217/fon.09.145
14. Doyen J, Trastour C, Ettore F, et al. Expression of the hypoxia-inducible monocarboxylate transporter MCT4 is increased in triple negative breast cancer and correlates independently with clinical outcome. *Biochem Biophys Res Commun*. 2014;451(1):54–61. doi:10.1016/j.bbrc.2014.07.050
15. Pertega-Gomes N, Felisbino S, Massie CE, et al. A glycolytic phenotype is associated with prostate cancer progression and aggressiveness: a role for monocarboxylate transporters as metabolic targets for therapy. *J Pathol*. 2015;236(4):517–530. doi:10.1002/path.4547
16. Boedtkjer E, Pedersen SF. The acidic tumor microenvironment as a driver of cancer. *Annu Rev Physiol*. 2020;82(1):103–126. doi:10.1146/annurev-physiol-021119-034627
17. Falsafi SR, Topuz F, Bajer D, et al. Metal nanoparticles and carbohydrate polymers team up to improve biomedical outcomes. *Biomed Pharmacother*. 2023;168:115695. doi:10.1016/j.biopha.2023.115695
18. Telegeev G, Kutsevol N, Chumachenko V, et al. Dextran-polyacrylamide as matrices for creation of anticancer nanocomposite. *Int J Polym Sci*. 2017;2017:4929857. doi:10.1155/2017/4929857
19. Yurchenko A, Nikitina N, Sokolova V, et al. A novel branched copolymer-containing anticancer drug for targeted therapy: in vitro research. *Bionanoscience*. 2020;10(1):249–259. doi:10.1007/s12668-019-00700-5
20. Chumachenko V, Virych P, Nie G, et al. Combined dextran-graft-polyacrylamide/zinc oxide nanocarrier for effective anticancer therapy in vitro. *Int J Nanomed*. 2023;18:4821–4838. doi:10.2147/IJN.S416046

21. Onishchenko AI, Prokopiuk VY, Chumachenko VA, et al. Hemocompatibility of dextran-graft-polyacrylamide/zinc oxide nanosystems: hemolysis or eryptosis? *Nanotechnology*. 2024;35(3):035102. doi:10.1088/1361-6528/ad02a3
22. Kutsevol N, Bezugla T, Bezuglyi M, Rawiso M. Branched Dextran- graft -polyacrylamide copolymers as perspective materials for nanotechnology. *Macromol Symp*. 2012;317–318(1):82–90. doi:10.1002/masy.201100087
23. Asahina K. Induction of cell death in pancreatic tumors by zinc and its fluorescence chelator TSQ. *Biol Trace Elem Res*. 2022;200(4):1667–1676. doi:10.1007/s12011-021-02770-7
24. Hübner C, Keil C, Jürgensen A, et al. Comparison of three low-molecular-weight fluorescent probes for measuring free zinc levels in cultured mammary cells. *Nutrients*. 2023;15(8):1873. doi:10.3390/nu15081873
25. Sápi J, Kovács L, Drexler DA, et al. Tumor volume estimation and quasi-continuous administration for most effective bevacizumab therapy. *PLoS One*. 2015;10(11):e0142190. doi:10.1371/journal.pone.0142190
26. Malatesta M. Histological and histochemical methods - theory and practice. *Eur J Histochem*. 2016;60:1.
27. Jouybari L, Kiani F, Akbari A, et al. A meta-analysis of zinc levels in breast cancer. *J Trace Elem Med Biol*. 2019;56:90–99. doi:10.1016/j.jtemb.2019.06.017
28. Lo S, Martins AF, Jordan VC, Sherry AD. Zinc as an imaging biomarker of prostate cancer. *Isr J Chem*. 2017;57(9):854–861. doi:10.1002/ijch.201700043
29. Renteria M, Belkin O, Aickareth J, et al. Zinc's association with the CmPn/CmP signaling network in breast cancer tumorigenesis. *Biomolecules*. 2022;12(11):1672. doi:10.3390/biom12111672
30. Saravanan R, Balasubramanian V, Swaroop Balamurugan SS, et al. Zinc transporter LIV1: a promising cell surface target for triple negative breast cancer. *J Cell Physiol*. 2022;237(11):4132–4156. doi:10.1002/jcp.30880
31. Karunasinghe N. Zinc in prostate health and disease: a mini review. *Biomedicines*. 2022;10(12):3206. doi:10.3390/biomedicines10123206
32. Liu Z, Lv X, Xu L, et al. Zinc oxide nanoparticles effectively regulate autophagic cell death by activating autophagosome formation and interfering with their maturation. *Part Fibre Toxicol*. 2020;17(1):46. doi:10.1186/s12989-020-00379-7
33. Baltaci AK, Yuce K, Mogulkoc R. Zinc metabolism and metallothioneins. *Biol Trace Elem Res*. 2018;183(1):22–31. doi:10.1007/s12011-017-1119-7
34. Kambe T, Tsuji T, Hashimoto A, Itsumura N. The physiological, biochemical, and molecular roles of zinc transporters in zinc homeostasis and metabolism. *Physiol Rev*. 2015;95(3):749–784. doi:10.1152/physrev.00035.2014
35. Maret W. Zinc in cellular regulation: the nature and significance of "zinc signals. *Int J Mol Sci*. 2017;18(11):2285. doi:10.3390/ijms18112285
36. Franklin RB, Ma J, Zou J, et al. Human ZIP1 is a major zinc uptake transporter for the accumulation of zinc in prostate cells. *J Inorg Biochem*. 2003;96(2–3):435–442. doi:10.1016/S0162-0134(03)00249-6
37. Holubova M, Axmanova M, Gumulec J, et al. KRAS NF-κB is involved in the development of zinc resistance and reduced curability in prostate cancer. *Metallomics*. 2014;6(7):1240–1253. doi:10.1039/c4mt00065j
38. Takatani-Nakase T. Zinc transporters and the progression of breast cancers. *Biol Pharm Bull*. 2018;41(10):1517–1522. doi:10.1248/bpb.b18-00086
39. Qu Z, Liu Q, Kong X, et al. A systematic study on zinc-related metabolism in breast cancer. *Nutrients*. 2023;15(7):1703. doi:10.3390/nu15071703
40. Zhang LY, Wang XL, Sun DX, et al. Regulation of zinc transporters by dietary flaxseed lignan in human breast cancer xenografts. *Mol Biol Rep*. 2008;35(4):595–600. doi:10.1007/s11033-007-9129-8
41. Chandler P, Kochupurakkal BS, Alam S, et al. Subtype-specific accumulation of intracellular zinc pools is associated with the malignant phenotype in breast cancer. *Mol Cancer*. 2016;15(1):2. doi:10.1186/s12943-015-0486-y
42. Kolenko V, Teper E, Kutikov A, Uzzo R. Zinc and zinc transporters in prostate carcinogenesis. *Nat Rev Urol*. 2013;10(4):219–226. doi:10.1038/nrurol.2013.43
43. Li D, Stovall DB, Wang W, Sui G. Advances of zinc signaling studies in prostate cancer. *Int J Mol Sci*. 2020;a21(2):667. doi:10.3390/ijms21020667
44. Anjum S, Hashim M, Malik SA, et al. Recent advances in zinc oxide nanoparticles (Zno nps) for cancer diagnosis, target drug delivery, and treatment. *Cancers*. 2021;13(18):4570. doi:10.3390/cancers13184570
45. Kadhim AA, Abbas NR, Kadhum HH, et al. Investigating the effects of biogenic zinc oxide nanoparticles produced using papaver somniferum extract on oxidative stress, cytotoxicity, and the induction of apoptosis in the THP-1 cell line. *Biol Trace Elem Res*. 2023;201(10):4697–4709. doi:10.1007/s12011-023-03574-7
46. Khan MS, Altwaijry N, Jabir NR, et al. Potential of green-synthesized ZnO NPs against human ovarian teratocarcinoma: an in vitro study. *Mol Biol Rep*. 2023;50(5):4447–4457. doi:10.1007/s11033-023-08367-8
47. Li Z, Yin X, Lyu C, et al. Zinc oxide nanoparticles induce toxicity in diffuse large B-cell lymphoma cell line U2932 via activating PINK1/Parkin-mediated mitophagy. *Biomed Pharmacother*. 2023;164:114988. doi:10.1016/j.biopha.2023.114988
48. Biswas A, Kar U, Jana NR. Cytotoxicity of ZnO nanoparticles under dark conditions via oxygen vacancy dependent reactive oxygen species generation. *Phys Chem Chem Phys*. 2022;24(22):13965–13975. doi:10.1039/D2CP00301E
49. Gong YN, Guy C, Olauson H, et al. ESCRT-III acts downstream of MLKL to regulate necroptotic cell death and its consequences. *Cell*. 2017;169(2):286–300. doi:10.1016/j.cell.2017.03.020
50. Zargarian S, Shlomovitz I, Erlich Z, et al. Phosphatidylserine externalization, "necroptotic bodies" release, and phagocytosis during necroptosis. *PLoS Biol*. 2017;15(6):e2002711. doi:10.1371/journal.pbio.2002711
51. Calianese DC, Birge RB. Biology of phosphatidylserine (PS): basic physiology and implications in immunology, infectious disease, and cancer. *Cell Commun Signaling*. 2020;18(1):41. doi:10.1186/s12964-020-00543-8
52. Wu N, Veillette A. Lipid scrambling in immunology: why it is important. *Cell Mol Immunol*. 2023;20(9):1081–1083. doi:10.1038/s41423-023-01009-w
53. Naeini MB, Bianconi V, Pirro M, Sahebkar A. The role of phosphatidylserine recognition receptors in multiple biological functions. *Cell Mol Biol Lett*. 2020;25(1):23. doi:10.1186/s11658-020-00214-z
54. Cunha A, Silva PMA, Sarmento B, Queirós O. Targeting glucose metabolism in cancer cells as an approach to overcoming drug resistance. *Pharmaceutics*. 2023;15(11):2610. doi:10.3390/pharmaceutics15112610
55. Khajah MA, Khushaish S, Luqmani YA. Lactate dehydrogenase A or B knockdown reduces lactate production and inhibits breast cancer cell motility in vitro. *Front Pharmacol*. 2021;12:747001. doi:10.3389/fphar.2021.747001
56. Li F, Xiang H, Pang Z, et al. Association between lactate dehydrogenase levels and oncologic outcomes in metastatic prostate cancer: a meta-analysis. *Cancer Med*. 2020b;9(19):7341–7351. doi:10.1002/cam4.3108

57. Li Z, Cui J. Targeting the lactic acid metabolic pathway for antitumor therapy. *Mol Ther Oncolytics*. 2023;31:100740. doi:10.1016/j.omto.2023.100740
58. Huang SS, Wu LY, Qiu Y, et al. Identification of lactate-related subgroups and prognostic model in triple-negative breast cancer. *J Cancer Res Clin Oncol*. 2023;149(14):13107–13122. doi:10.1007/s00432-023-05171-6
59. Alarifi S, Ali D, Alkahtani S, et al. Induction of oxidative stress, DNA damage, and apoptosis in a malignant human skin melanoma cell line after exposure to zinc oxide nanoparticles. *Int J Nanomed*. 2013;8:983–993. doi:10.2147/IJN.S42028
60. Morsy S, Abd-Ellatif RN, Soliman NA, Ibrahim WM. Bioenergetic signature as a target of zinc oxide nanoparticles in Ehrlich ascitic carcinoma-bearing mice. *J Biochem Mol Toxicol*. 2021;35(2):e22647. doi:10.1002/jbt.22647
61. Haque M, Konthoujam I, Lyndem S, et al. Formation of ZnS quantum dots using green tea extract: applications to protein binding, bio-sensing, anti-bacterial and cell cytotoxicity studies. *J Mater Chem B*. 2023;11(9):1998–2015. doi:10.1039/D2TB02265F
62. Shim KH, Hulme J, Maeng EH, et al. Analysis of zinc oxide nanoparticles binding proteins in rat blood and brain homogenate. *Int J Nanomed*. 2014;9(Suppl 2):217–224. doi:10.2147/IJN.S58204
63. Žukiene R, Snitka V. Zinc oxide nanoparticle and bovine serum albumin interaction and nanoparticles influence on cytotoxicity in vitro. *Colloids Surf B Biointerfaces*. 2015;135:316–323. doi:10.1016/j.colsurfb.2015.07.054
64. Singh U, Saifi Z, Kumar M, et al. Role of structural specificity of ZnO particles in preserving functionality of proteins in their Corona. *Sci Rep*. 2021;11(1):15945. doi:10.1038/s41598-021-95540-3
65. Krug HF, Wick P. Nanotoxicology: an interdisciplinary challenge. *Angew Chem Int Ed*. 2011;50(6):1260–1278. doi:10.1002/anie.201001037
66. Arab-Bafrani Z, Zabihi E, Jafari SM, et al. Enhanced radiotherapy efficacy of breast cancer multi cellular tumor spheroids through in-situ fabricated chitosan-zinc oxide bio-nanocomposites as radio-sensitizing agents. *Int J Pharm*. 2021;605:120828. doi:10.1016/j.ijpharm.2021.120828
67. Dubey P, Sertorio M, Takiar V. Therapeutic advancements in metal and metal oxide nanoparticle-based radiosensitization for head and neck cancer therapy. *Cancers*. 2022;14(3):514. doi:10.3390/cancers14030514
68. Alavi N, Maghami P, Fani Pakdel A, et al. The advance anticancer role of polymeric core-shell ZnO nanoparticles containing oxaliplatin in colorectal cancer. *J Biochem Mol Toxicol*. 2023;37(5):e23325. doi:10.1002/jbt.23325
69. Yan G, Huang Y, Bu Q, et al. Zinc oxide nanoparticles cause nephrotoxicity and kidney metabolism alterations in rats. *J Environ Sci Health A Tox Hazard Subst Environ Eng*. 2012;47(4):577–588. doi:10.1080/10934529.2012.650576
70. Chen A, Feng X, Sun T, et al. Evaluation of the effect of time on the distribution of zinc oxide nanoparticles in tissues of rats and mice: a systematic review. *IET Nanobiotechnol*. 2016;10(3):97–106. doi:10.1049/iet-nbt.2015.0006
71. Kausar S, Jabeen F, Latif MA, Asad M. Characterization, dose dependent assessment of hepatorenal oxidative stress, hematological parameters and histopathological divulging of the hepatic damages induced by Zinc oxide nanoparticles (ZnO-NPs) in adult male Sprague Dawley rats. *Saudi J Biol Sci*. 2023;30(9):103745. doi:10.1016/j.sjbs.2023.103745
72. Yao Y, Zang Y, Qu J, et al. The toxicity of metallic nanoparticles on liver: the subcellular damages, mechanisms, and outcomes. *Int J Nanomed*. 2019;14:8787–8804. doi:10.2147/IJN.S212907
73. El-Maddawy ZK, Abd El Naby WSH. Protective effects of zinc oxide nanoparticles against doxorubicin induced testicular toxicity and DNA damage in male rats. *Toxicol Res*. 2019;8(5):654–662. doi:10.1039/c9tx00052f
74. Elgohary A, Metwalli F, Mostafa NY, et al. Zinc oxide nanoparticles regulate NF-kB expression and restrict inflammation response in doxorubicin-induced kidney injury in rats. *Toxicol Environ Health Sci*. 2023;15(4):437–448. doi:10.1007/s13530-023-00194-5
75. Hassan HFH, Mansour AM, Abo-Youssef AMH, et al. Zinc oxide nanoparticles as a novel anticancer approach; in vitro and in vivo evidence. *Clin Exp Pharmacol Physiol*. 2017;44(2):235–243. doi:10.1111/1440-1681.12681
76. Mahdizadeh R, Homayouni-Tabrizi M, Neamati A, et al. Green synthesized-zinc oxide nanoparticles, the strong apoptosis inducer as an exclusive antitumor agent in murine breast tumor model and human breast cancer cell lines (MCF7). *J Cell Biochem*. 2019;120(10):17984–17993. doi:10.1002/jcb.29065
77. Goel A, Dani V, Dhawan DK. Zinc mediates normalization of hepatic drug metabolizing enzymes in chlorpyrifos-induced toxicity. *Toxicol Lett*. 2007;169(1):26–33. doi:10.1016/j.toxlet.2006.07.342
78. Grüngreiff K, Reinhold D, Wedemeyer H. The role of zinc in liver cirrhosis. *Ann Hepatol*. 2016;15(1):7–16. doi:10.5604/16652681.1184191